The role of iron in inflammatory oligodendrocyte pathology:

From clinical to cell culture

by

Erika Bose Johnson

A thesis submitted in partial fulfillment of the requirements for the degree of

Master of Science

Center for Neuroscience

University of Alberta

Abstract

MS is a chronic demyelinating disease of the CNS that presents with debilitating symptoms in the later stages of disease progression and therefore a high demand for targeted disease-modifying treatments exists. In order to create effective treatments the causalities between the symptoms and pathological mechanisms of the disease need to be properly understood. One such area that remains poorly understood is the role of excess iron deposition in disease aetiology and progression. Literature has shown excess iron deposition in the brains of those with MS. However, whether it is the concentration of excess deposition, the brain-specific regions of deposition, or even the method of iron deposition/metabolism that causes this excess deposition is not understood. This thesis presents a set of experiments that observe the possible role of iron on inflammatory oligodendrocyte pathology, from a macro-to a micro-level. First, the deposition pattern of iron in regards to gross anatomy in brains affected by MS is observed and quantified using MRI images as well as tissue samples. The data presented here suggests that both the severity and/or maturity of the lesion play a role in the level of excess and pattern of iron deposition. Second, a set of experiments are performed that manipulate a pathway crucial to iron homeostasis as well as a group of receptors implicated in the disease progression of MS (HO-1 and P2X respectively) to elucidate possible synergistic activity between them. The results suggest an association between the purinergic receptors and the HO-1 pathway.

Preface

This thesis contains both independent and collaborative work. No publications yet

The research in this thesis was conducted under the supervision of Dr. Kathryn Todd. The research presented in Chapter Two was formulated together with the team of scientists who helped me along the way as well as on my own. The research presented here encompasses a wide degree of interests including both in-vitro and clinical studies. It has been through the collaboration with the Department of Medicine, the NRU, the NMHI, and Pathology team that inspired me to ask further questions.

Acknowledgements

I would like to express gratitude to the members of my committee, Dr. Alan Wilman and Dr. Ian Winship, for their time and input in reviewing this thesis. I would also like to thank Kim Wong and Jocelyn Madeira for the technical assistance that they provided. Additionally, I would like to thank Dr. Matthew Churchward for the endless guidance, feedback, and patience. Finally, I would like to thank Dr. Kathryn Todd for the invaluable supervision, guidance, and mentoring that she has provided.

Table of Contents

List of Figures

List of Abbreviations

ANOVA
Analysis of Variance
ATP
Adenosine Triphosphate
BCA
Bicichonic Acid
C2
CORM-2
CC3
Cleaved Caspase-3
CNPase
2'3'-Cyclic-nucleotide 3'-phosphodiesterase
CNS
Central Nervous System
CO
Carbon Monoxide
CORM-2
Carbon Monoxide Releasing Molecule 2
DAMP
Damage Associated Molecular Pathway
DAPI
4,6-Diamindino-2-phenylindole
DMT
Disease Modifying Therapy
DNA
Deoxyribonucleic Acid
EAE
Experimental Autoimmune Encephalomyelitis
EC50
Half Maximal Effective Concentraion
EDTA
Ethylenediaminetetraacetic Acid
ELISA
Enzyme-linked Immunosorbent Assay
FOI
Feature of Interest
GFAP
Glial Fibrillary Acidic Protein
HO-1
Heme Oxygenase-1
Iba-1
Ionized Calcium-Binding Adaptor Molecule-1
IFN
Interferon
IL-1B
Interleukin 1-beta
LDH
Lactate Dehydrogenase
MBP
Myelin Basic Protein
MG
Microglia
MRI
Magnetic Resonance Imaging
MS
Multiple Sclerosis
NBM
Neurobasal media
NLRP3
NACHT, LRR, AND PYD domains-containing protein 3
NPC
Neural progenitor Cells
O4
Oligodendrocyte Marker O4
OLG
Oligodendrocyte
Olig2
Oligodendrocyte Transcription Factor-2
OPC
Oligodendrocyte Precursor Cell
PAMP

Pathogen Associated Molecular Pathway

PBS
Phosphate Buffered Saline

PDGF
Platelet-derived Growth Factor

PPMS
Primary Progressive MS

PRMS
Progressive Relapsing MS

RCD
Regulated Cell Death

ROI
Region of Interest

ROS
Reactive Oxygen Species

RRMS
Relapsing-Remitting MS

SnPP
Tin Protoporphyrin

SPMS
Secondary Progressive MS

T3
Triiodothyronine

TLR
Toll-like Receptor

TNF
Tumor Necrosis Factor

Chapter One

Introduction

1.0 Multiple Sclerosis

Multiple sclerosis (MS) is a demyelinating autoimmune disorder of the CNS that affects 2.5 million people worldwide[1,2]. The prevalence of MS increases with increasing distance from the equator, with Canada being the country with the highest prevalence[3]. The emergence of symptoms, and thus diagnosis, is most common between the ages of 20 and 40. In order to give a diagnosis of MS three criteria must be met: the appearance of symptoms (typically initially presenting as anesthesia and parathesia), the presence of lesions within the CNS (demonstrated by magnetic resonance imaging (MRI)), as well as analysis of the cerebrospinal fluid (CFS) for oligoclonal bands. Once the diagnosis has been made the progression of the disease will vary according to the type of MS the patient has. There are four types of MS: relapsing-remitting (RR-MS), secondary progressive (SP-MS), primary progressive (PP-MS), and progressive relapsing (PR-MS). The distinction between the types of MS lies with the intensity and temporal distribution of flare-ups. More information on the distinctions between the types is given in Chapter 2.

The brain attacking itself characterizes the pathology of MS. Specifically, the immune cells of the central nervous system (CNS) target and degrade the myelin sheaths produced by the oligodendrocytes, which produce a lesion. A lesion is identified using MRI techniques and, depending on the specific technique used, will either appear as a region of hypointensity in the brain (T1-weighted MRI), or a region of hyperintensity in the brain (FLAIR MRI, axial diffusion-weighted MRI, and T2-weighted MRI)[4–6]. These

lesions lead to a reduction, and eventually loss, of brain signals that underlie movement, sensation, and even cognitive functioning.

Lesions are characterized in two different ways[7–9]. First, by their inclusion of immune cells and the presence of viable neuronal axons (i.e. based on their stage of inflammatory destruction). Within this framework are acute active lesions, chronic active lesions, inactive lesions, and shadow plaques. Acute active lesions are those that are newly formed, they contain demyelination throughout the lesion, infiltration of immune cells, no glial scarring, and although neuronal axons are spared widespread axonal damage is observed. Chronic active lesions are those that are older in age, have a central region of hypocellularity, complete loss of oligodendrocytes, extensive demyelination, glial scarring along the lesion border, and activity of immune cells is limited to the border of the lesion. Inactive lesions refer to lesions that are older and share many of the same characteristics with chronic active lesions, with their distinction lying in a lack of any inflammatory cellular activity either within the center or the border of the lesions. In opposition to all of the above, a shadow plaque is a lesion that has undergone remyelination, therefore there are both neuronal axons and oligodendrocytes to be found, with few activated macrophages/microglia.

The second method of characterizing lesions is according to their location within the brain[7,9]. Within this characterization lesions are labeled as either Type I, Type II, or Type III. Type I lesions are those that have a leucocortical location and involve the gray matter as well as the adjacent white matter. Type II lesions are located only on the cortex. Type III lesions extend from the pial surface and also run parallel to the pial surface. Type III lesions are noteworthy for the fact that they occur specifically in gray matter of

the brain, when MS is typically characterized by the destruction of the myelin that composes the white matter of the brain. The mechanisms behind Type III lesions remain unknown.

The cause of MS remains unknown, however certain risk factors have been identified. These risk factors include: genetics, age, sex, race, climate, and certain infections[1–3]. More specifically MS most commonly affects people between the ages of 20 and 40, women are twice as likely to be diagnosed with MS than men, if someone in your family has MS you are more likely to develop it, contracting the Eppstein-Barr virus earlier in life can increase your susceptibility to MS later in life, people of Northern European descent are most likely to be diagnosed with MS, similarly MS is much more common in countries with temperate climate. It remains unclear whether the different types of MS are associated with different risk factors, whether the risk factors work together in multiplicative ways to increase risk, or whether one risk factor is dominant over others.

1.1 Iron in MS

Iron plays an integral role in the healthy functioning of our brains, including for synthesis of neurotransmitter, as a required factor for the synthesis of DNA, and as an integral component in the production of myelin[10]. Many of its functions are involved in maintaining homeostatic metabolism in the brain. However, when not tightly regulated iron can become harmful to the brain in excess concentrations[11–14]. Most often iron is found in a form that is bound to either iron transport or storage proteins. When it is bound to storage or transport proteins (transferrin or ferritin respectively) it is prevented from initiating damage on its immediate environment. Contrary to the neutral nature of bound iron, iron that is free is extremely reactive. In this form iron is able to catalyze reactions

that create reactive oxygen species (ROS) that promote cellular damage on many levels. Iron-dependent ROS have been implicated in various diseases such as Alzheimer's[15–21], Parkinson's[22–30], Huntington's[31–39], general neurodegeneration[11,12,14,40–44], and is currently being highly researched as a possible pathological mechanism in Multiple Sclerosis (MS)[15,45,46,46–56].

1.2 Localization of Iron in MS

To further understand the role abnormal iron deposition may play within the disease pathology of MS, it is important to also understand how it is localized differently within the diseased brain compared to the healthy brain. In addition to being a vital component of normal cellular functioning as mentioned above, it is also naturally localized at higher concentrations in certain brain regions, as well as steadily increasing in the healthy aged brain from around 50 years old. Specifically, within the healthy brain high levels of iron are found within deep gray areas such as the Substantia Nigra and the Basal Ganglia. At a cellular level, iron is typically concentrated within oligodendrocytes and the associated myelin sheath in healthy brains. On the contrary, within brains from individuals with MS, abnormally high iron levels have been observed in both gray and white matter areas. This means that in addition to the areas in which high iron levels are expected, it is also seen in white matter such a the centrum semiovale[57], as well as abnormally high concentrations in deep gray nuclei such as globus pallidus, thalamus, and putamen[11–13]. Interestingly, abnormal accumulation of iron deposition has been linked to disease progression in MS. Specifically, a correlation is observed between atrophy in deep gray nuclei and increased disease progression[45]. New MRI techniques have allowed excess iron deposition to be identified, localized, and quantified as a function of their volume within the brain. Deep gray areas hold significance within the

symptomatology of MS as one of their main roles is modulating motor function, and retardations of motor abilities is a primary symptom of the disease progression of MS. The use of MRI techniques has shown that the presence of abnormally high iron deposition in the deep gray areas early in the disease progression is a better predictor of disease course and disability levels than other markers of disease[45,46,52,54,56,59,60].

Despite the useful nature of MRI techniques in foretelling disease course and severity, they are not yet sensitive enough to suggest correlations of region-specific iron deposition to cellular specific iron patterns. Namely, Type III lesions are undetectable using these techniques[61]. As mentioned earlier, these lesions are located in the grey matter of the cortex, which suggests the pathology of MS is a CNS-wide disorder, rather than a white-matter-specific-disorder. Interestingly, Type III lesions are observed early on in the disease progression, but due to the difficulty visualizing them, little research has been conducted on how they contribute to disease progression. As a consequence, we are unable to determine whether the region-specific levels of excess iron deposition can be associated with any of the pathological cellular mechanisms that are associated with the disease progression of MS. The inability to draw such correlations suspends the capability to identify the initiating factor or event underlying this disease.

Understanding the localization pattern that underlies excess iron deposition in MS could help us understand the functional dysregulations that cause it. When we are able to understand why deep gray areas, or motor areas are the primary targets for excess iron deposition we may be able to understand the mechanisms that cause the distinction between these and other brain areas, which could further help us understand the specific set of mechanisms underlying the general aetiology and pathology of MS.

1.3 Micro Localizations of Iron

Within the realm of MS research a great deal of interest is focused on the brain regions associated with the abnormal iron depositions. The reason behind this is two-fold: on one hand it is because a correlation exists between iron deposition observed in deep gray nuclei and disease progression, on the other hand it is due to the fact that there are reports of increased iron deposition within active lesions which is no longer observed in inactive/chronic lesions[46,49,52,54,55]. This suggests that iron is implicated in disease progression. However the mechanisms behind the excessive deposition, as well as the knowledge of whether the iron is a cause or effect of the disease remains unclear. Determining the regions of iron deposition within the microenvironments in these brain regions present an important step in creating wider understanding on the role of iron in MS.

The work presented here looks at both the macro- and the micro-levels of abnormal iron deposition. On the micro-level scale, understanding whether certain brain regions have a tendency to have abnormal iron depositions either intra-cellular or peri-cellular is important. Namely, this difference points to the types of damage the cells, and concurrently the brain region, may be undergoing

1.3.1 Role of Intracellular Excess Iron

Within the cell, iron is preferentially taken-up, and stored by the mitochondria[13,14,44,62,63]. This is of particular importance for three different reasons. To begin with, the mitochondrion is one of the main sites of ROS production, and excess iron has been shown to drastically increase the levels of ROS production. In addition, the mitochondrion requires very tightly regulated iron levels in order to run and function normally. Second, the mitochondrion is the regulator of the intrinsic death pathway,

leading to apoptosis. Third, mitochondrial dysfunction has been shown to play a role in the disease pathology of MS as well[64,65].

The convergence of these roles is noteworthy as they have been shown to play a role in the disease pathology of MS. Of particular note is the storage of iron. As mentioned previously, abnormal iron deposition has shown to be increasingly associated with the disease progression of MS. Although many of the dyregulated functions that contribute to the disease progression of MS are known, the lack of knowledge surrounding its aetiology has created an inability to produce both precisely targeted disease-modifying treatments as well as any hopes of discovering a cure. Therefore uncovering new cellular dysfunctions and dysregulations that exist within MS, as well as further understanding how the various understood dysfunctions and dysregulations interact with each other to create a disease timeline, may elucidate the aetiology of this crippling disease. The research presented in this paper falls under the latter category, in which mechanistic dysfunctions/dysregulations are examined with respects to the possible existence of synergistic activity and cross-talk, and how this may affect disease progression. This thesis begins by looking at the macro-level of abnormal iron deposition, and ends with a micro-level look at how this iron dysregulation may be occurring as well as how this may be interacting with other known factors of the disease to exacerbate neuroinflammation.

1.3.2 Role of Iron in Ferroptosis

In 2012 a new form of regulated cell death (RCD) was discovered and coined ferroptosis[66]. Ferroptosis is an iron-dependent RCD that differs significantly from apoptosis and necrosis in its morphologically, molecular biology, induction and inhibition, as well as its signaling pathway[11,67–73]. Ferroptosis is noteworthy for the

context of this research as it is suggested that ROS- and iron-dependent signaling are required for the induction of ferroptosis. Therefore not surprisingly, the HO-1 pathway which plays a critical part in the metabolism and homeostasis of iron, has been found to be highly involved in the induction of ferroptosis. Specifically, with its agonism increasing the occurrence of ferroptosis and its antagonism inhibiting its occurrence[74]. Similarly to the diseases excess iron levels have been implicated in, Ferroptosis has been found to play a role in Alzheimers, Parkinsons, and general neurodegeneration. The increasing knowledge of the mechanisms and implications of Ferroptosis make it a form of RCD that may be highly relevant to the disease progression and pathology of MS.

1.4 Layout of the Thesis

This thesis takes a both macro- and micro-approach with respects to its focus on investigating the parameters of excess iron deposition and their respective roles in the disease progression. It begins with a macro-approach observing the abnormal localization of iron in patients. This first section follows patients temporally in a way that is not often seen to allow for a full picture of both the accumulation of iron within the whole brain, as well as patterns of accumulations within target brain regions. The transition from human research to cell culture research occurred in order to address mechanistic questions regarding abnormal iron deposition patterns. Second, we characterized a line of rat immortal oligodendrocytes that have remained largely uncharacterized and therefore underutilized. Third, we created a co-culture model to represent the basic cell interactions (micro-approach) that are observed in the early stages of the neurodegeneration and neuroinflammation in MS. This co-culture model was then pharmacologically manipulated with agonists and antagonists of the receptors of the purinergic family as well as the HO-1 pathway to determine the existence of synergistic activity and cross talk

between them. Finally we discuss how our findings have added to the knowledge of abnormal iron deposition within MS and where we would like to take future research.

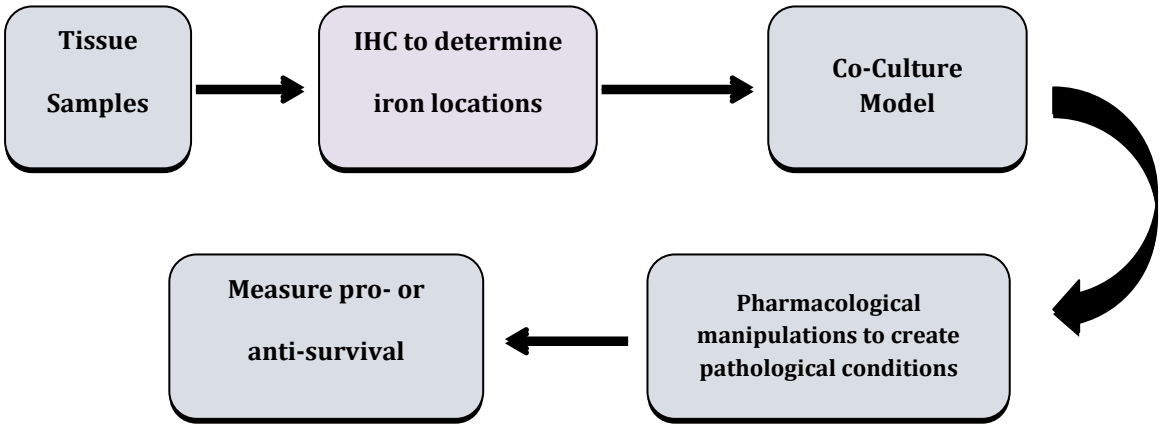

Figure 1-1. A flowchart depicting the outline of the experiments included in this thesis.

CHAPTER TWO

A STUDY OF IRON LOCALIZATION IN BRAINS WITH MS: MULTI-LEVEL ANALYSIS FROM MRI TO QUANTIATIVE HISTOLOGICAL EXAMINATION

1.0 Abstract

MS is a chronic demyelinating disease of the CNS that presents with debilitating symptoms in the later stages of disease progression and therefore a high demand for targeted disease-modifying treatments exists. In order to create effective treatments the causalities between the symptoms and pathological mechanisms of the disease need to be properly understood. One such area that remains poorly understood is the role of excess iron deposition in disease aetiology and progression. Literature has shown excess iron deposition in the brains of those with MS[45,47,50]. However, whether it is the concentration of excess deposition, the brain-specific regions of deposition, or even the method of iron deposition/metabolism that causes this excess deposition is not understood. To date the majority of research has used two populations of human subjects: one for the pre-mortem MRI images, and a different one for the post-mortem tissue collection. Thus, the conclusions drawn from previous research remains speculative when addressing causality with regards to its aetiology and progression. In addition, when addressing micro-level iron quantification a qualitative, subjective methodology is often used. In this paper we use a consistent patient pool to conduct a variety of experiments in regards to excess iron deposition in MS. We describe a set of five analyses that address the localization and quantification of region–specific iron levels: MRI-imaging to identify lesions and iron-rich brain regions, pathology reports identifying lesions and other brain abnormalities, a

myelin stain to determine areas of demyelination, a ferric stain to determine iron deposition at a cellular level, and finally a computerized identification and quantification of the iron identified in the previous analysis. The data presented here suggests that both the severity and/or maturity of the lesion play a role in the level of excess and pattern of iron deposition. Additionally, these data demonstrate that type of disease as well as disease severity may affect both whole-brain as well as region-specific iron deposition.

1.1 Introduction

Multiple Sclerosis (MS) is a debilitating immune disorder of the Central Nervous System (CNS) and is characterized by demyelination. Initially, MS often presents as sensory abnormalities, which progress to include motor abnormalities in later stages. Eventually this leads to a loss of sensory, motor, cognitive, and even affective behaviours.

Although the final stages appear similar, the progression of the disease is variable depending on the type of MS the patient has. Types of MS are: relapsing-remitting (RRMS), secondary-progressive (SPMS), primary-progressive (PPMS), and progressive-relapsing (PRMS)[1]. The key differences between types exist in the severity of flare-ups, degree and length of remission between flare-ups, and accumulation of disability. Often, patients are given an initial diagnosis of RRMS, which becomes SPMS. RRMS is one of the more manageable forms of MS as flare-ups are mild with full and lengthy remissions in-between, and accumulation of disability is minimal until the later stages. In contrast, PPMS and PRMS are both types of MS that are severe from the onset. They are characterized by relentless flare-ups, little to no remission periods, and steady

accumulation of disability over a short period of time. Given the inadequate knowledge of the aetiology of this disease (outlined in Chapter 1), it is not clear if all types share similar dysfunctional mechanisms or if diverse mechanisms create the variation observed between types.

Despite the unknown aetiology of the disease, the main pathological actions are known. MS is the result of the degradation of myelin, degeneration of oligodendrocytes, as well as the degeneration of associated neuronal axons. The initial target appears to be the myelin sheath[2-4], a lipid-rich substance that wraps around neuronal axons and is produced by oligodendrocytes. Myelin performs beneficial roles including increasing signal fidelity and speed of neural firing, protecting neuronal axons from damage, and providing energy directly to the axons[5], as well as facilitating motor learning [6]. The supportive role myelin plays towards neurons is crucial as neurons propagate an electrical signal that underlies all human behaviour. Accordingly, the integrity of the affected behaviours steadily decline with increasing demyelination.

Controversy surrounds the nature of MS, with two main theories competing for the causal role. The first theory is the widely proclaimed autoimmune theory, which holds that MS is the result of a targeted immune attack against the myelin of the brain. However, MS does not fulfill the requirements to be considered an autoimmune disease. Specifically, no precise autoantigen has yet been identified in all patients[75–77]. The majority of the claim of MS being an autoimmune disease originates from animal models such as experimental autoimmune encephalomyelitis (EAE) and acute disseminated encephalomyelitis (ADEM), which have been widely shown to differ from MS in the nature of their lesions and even disease course[78].

The second theory is that the pathology observed in MS is virus-induced. Research has exhibited a high correlation with MS to viruses such as infectious mononucleosis (IM)[79–81] and Eppstein-Barr virus (EBV)[82]. Further support for this theory is that various species-specific viruses produce very similar results: canine distemper virus in dogs, JHM and MHV-4 virus in mice, and visna virus in goats [83].

1.1.1 Iron in MS

Iron plays an important role in normal brain metabolism; it is involved in processes such as myelination and oxidative phosphorylation[11,84,85]. Within the physiologically "normal" brain iron is often stored as non-heme iron within oligodendrocytes (OLGs) and myelin. Ferritin is often associated with non-haem iron as it is an intracellular iron-binding protein, which functions to store, as well as control the release, of iron. Given that, when iron is not associated with a storage or transport protein, it is considered free iron. It is important to realize that in this form it is able to participate in chemical reactions, which produce reactive oxygen species (ROS). In controlled concentrations ROS play an integral role in cell signalling and provide a link to the adaptive immune system. However, in excess ROS become toxic to the cell[11,84,85]. Some of the damaging effects induced by excess ROS include: DNA damage, lipid peroxidation, oxidation of amino acids, and oxidatively deactivating specific enzymes. Unchecked ROS release has been implicated in the progression of diseases such as cancer, Alzheimer's Disease, Diabetes Mellitus, and even obesity[7] . (Citation)

Similarly, abnormal iron deposition is observed in the disease pathology of MS. It is not clear if it plays the role of cause or effect concerning disease on-set and progression. This abnormality has been found in both white and gray matter areas, and can present as different patterns of deposition. The observations accumulated thus far

motivate research avenues to increase the field's knowledge on the specifics underlying the mechanics of this pathology. Creating a therapeutic target for abnormal iron deposition requires us to be able to determine with high specificity and certainty what aspect of the mechanism should be targeted: e.g., inhibiting iron accumulation, blocking toxic activity of iron, enhancing iron removal, or even inhibiting downstream pathogenic effects in other signalling pathways.

1.1.2 Iron Location Patterns in Abnormal Deposition

Iron can be found either bound to storage or transport proteins, or unbound in a labile form. Within this labile form the iron readily converts hydrogen peroxide into free radicals. Iron toxicity occurs when the ratio of free iron to iron-binding tranferrin is too high, which means that there is a lack of required transferrin receptors to bind all of the unbound iron. This causes the iron to remain in the labile iron pool and freely move around within the neuropil, therefore able to initiate and perpetuate ROS-mediated damage. Determining whether excess iron is associated with cells or other cellular architecture, or existing in a labile form is important in understanding the roles it can play in neurodegeneration and inflammation. When the excess iron is seen this could lead to apoptosis, necrosis, or even ferroptosis.

There are two families of work on iron in MS that remain unconnected; we will briefly discuss each of them. First, there is the body of research formed by using post-mortem paraffin-embedded tissue with previous patient medical records indicating regions of interest and disease severity. The work done here has been largely descriptive in nature, focusing on the patterns of distribution in both whole-brain and region-specific patterns[16,18]. Indeed, this research demonstrated an increase in iron deposition at the perimeters of active lesions. In contrast, chronic or remyelination lesions did not show

this increase. Furthermore, abnormally deposited iron is typically found in one of two locations: as extracellular deposits in the neuropil, or accumulated within/closely associated with cell bodies. Patterns of iron deposition differ significantly between white matter and gray matter areas.

Second, there is the knowledge that has been gained through MRI imaging methods of iron identification. It has been broad in nature as it works with living patients and can follow the progression of iron deposition throughout the disease course, as well as possible effects on accumulation of disability[19,15]. For instance, this research demonstrated a higher iron load in deep gray nuclei compared to other brain regions[14,16,17]. Moreover, it elucidated a correlation between atrophy in deep gray nuclei (e.g., caudate nucleus, pulvinar, and putamen) and increased disease progression[15].

Additionally excess iron deposition is displayed as a lower signal on a T2 MRI scan. Correspondingly, disease progression and intensity is correlated with T2 low-signal regions, with higher levels being reported in SPMS compared to RRMS. Together with the differences of deposition patterns between gray and white matter, these results provide compelling evidence that multiple mechanisms may be involved. Consequently these advancements present the ability to begin to look at iron deposition as a marker of disease progression.

Considering the aforementioned bodies of work, there is an open avenue of investigation to establish correlation between localization of iron, pattern of iron deposition, and disease progression. A key limitation of previous findings in this area is that a contiguous patient pool is not used for both the MRI scans and the post-mortem tissue analysis. This presents a problem, as MRI images cannot differentiate between

bound and unbound iron, whether it is intracellular or extracellular. Without a contiguous patient dataset it is not possible to correlate results about disease or lesions severity/progress, iron deposition by MRI at a whole brain level, and the patterns of iron deposition at a cellular level. This confounds an analysis of whether iron accumulation is a causal factor in damage seen in MS lesions or is a phenomenological observation. We propose to examine, in a contiguous patient dataset, the relationships between iron deposition in deep gray regions (via MRI), and cellular patterns of both iron deposition and lesional damage with an aim of improving our understanding of the potential role of iron in the neuropathology of MS. This will be done using a contiguous patient pool to compare MRI scans (looking at macro levels of iron and myelin patterns), pathology reports, and sections stained for micro-levels of myelin and iron deposition patterns.

Furthermore, a common issue is faced with quantifying iron levels on a cellular level, which lies with the fact that it predominantly relies on subjective quantification reports of either pathologists or scientists. This has been difficult to automate due to the wide variety of shades encompassed within the positive-iron stained regions. We have therefore also created an objective, protocol-specific quantification program that determines iron-load in a region-specific manner.

1.2 Methods

1.2.1 Subjects

Subjects used were the same subjects used in collaborative work from Walsh et al., 2013[86]. Institutional ethical approval was obtained, as well as informed consent from either the patients themselves or their families. Briefly, 4 deceased subjects diagnosed

with MS were included in this study, as well as 1 control patient. In all MS subjects, neurologists who specialize in MS made the diagnosis of MS. In addition, three neuropathologists confirmed the diagnosis.

Of the MS patients, MRI images were obtained for 3 of the 4 within 28 hours post-mortem. The remaining MS patient had MRI images taken within a year proceeding death. The subjects were not age-matched or gender-matched and died due to various complications of MS. The control patient died due to rheumatic heart disease. The work-flow described in section 1.1.2 was conducted post-mortem.

1.2.1 Sectioning

Regions of the brains containing lesions were identified, dissected, and embedded in 18% formalin by pathologists, following which we received the pre-chosen brain regions. The brains regions were then sectioned into 11 um slices. The degree of pathology varied between the patients with MS, ranging from chronic primary MS to secondary progressive MS.

1.2.2 MRI Imaging

The MR images were acquired and processed according to the procedure outlined by Walsh et al., 2013. Briefly, a 4.7-T whole-body imaging system was used. Four axial MR imaging techniques were run and compiled to create the MR imaging protocol: standard T2-weighted fast SE, R2* mapping, R2 mapping, and phase imaging.

1.2.3 Histological Staining

Weil's myelin histology was performed to corroborate the MRI images and to histologically visualize the extent of myelin presence in the brain tissue sections. The protocol requires the reduction of a salt by myelin and therefore results in the visualization of the protocol in myelin-rich areas. In addition, this protocol affords a clear

visualization of areas of demyelination in regards to gross anatomy. Slide-mounted sections were briefly heated to melt the paraffin wax, deparaffinized in xylene and then brought through a decreasing series of ethanol dilutions to re-hydrate the tissue. Preparation of the Weil's staining solution was completed as follows: 10% hematoxylin (Sigma, H3136) in ethanol was allowed to ripen for 1 week and then diluted at 1:4 with distilled water prior to use. The staining solution was made up of equal parts of the diluted hematoxylin solution and 4% ammonium iron (III) sulfate (Sigma, 221260) which was heated to 55°C prior to application. Sections were stained with the Weil's staining solution at 55°C for 45 minutes, cleared in tap water and then macroscopically differentiated with 4% ammonium iron (III) sulfate at room temperature until the background turned gray in colour. Following several washes in tap water, Weigert's microscopic differentiator [1% borax (Fisher, S249) and 1.25% potassium ferricyanide (Sigma, P230)] was applied to the sections and monitored under a microscope until the myelin developed a deep blue hue and the background turned cream in colour. Sections were subsequently washed with tap water, cleared with double distilled water and mounted with Fluoromount G (Southern Biotech, 0100-01).

Iron Staining was performed on adjacent sections to corroborate the MRI images and to determine the presence of iron in the brain tissue. Briefly, sections followed the same deparaffinization and rehydration procedure as indicated above for the Weil's histology. To prevent false positive staining from the residue of any metal lab equiptment, special care was taken to avoid contact with metal and as a result, the entire protocol was performed using double distilled water, glass, wood, and plastic lab equipment. Sections were incubated for 20 minutes in working potassium-hydrochloric

acid solution [2% potassium ferrocyanide (Sigma, P3289) and 2% hydrochloric acid], followed by several washes with double distilled water, and counterstained for 1 minute with 1% neutral red (Sigma, 72210) made in 0.1% acetic acid. Sections were subsequently cleared in double distilled water, dehydrated with increasing grades ethanol into xylene and then mounted with Permount (Fisher, SP15).

1.2.4 Immunofluorescence

Immunostaining was performed using antibodies against glial fibrillary acidic protein (mouse anti-GFAP [1:500] Sigma, G3893), Iba1 (rabbit anti-Iba1 [1:500] Wako, 01-1974), and Ferritin (rabbit anti-ferritin [1:500] Abcam, ab7332) in order to visualize the astrocytic, microglia, and ferritin composition of the tissue respectively. Briefly, paraffin sections followed the same deparaffinization and rehydration procedure as described in the above Weil's histology. An antigen retrieval step was used to break protein cross-links formed during fixation and to improve primary antibody penetration. The antigen retrieval step involved immersing the slide-mounted sections into a boiling (95-100°C) solution of Ethylenediaminetetraacetic Acid (EDTA) (1mM EDTA (EM Sciences, B10093-30), 0.05% Tween 20 (Sigma, P-5927), adjusted to a pH of 8.0 (Fisher Scientific, Accumet Basic AB15) for 30 minutes, after which the sections remained in the cooling EDTA solution for 15 minutes. Sections were subsequently cleared with phosphate buffered saline (PBS), followed by washes of double distilled water. Prior to primary antibody application, sections were blocked for 1 hour with 0.4% Triton X-100 (Fisher-Scientific, BP151) in universal blocking serum (Dako, X0909). The primary antibodies were diluted into a buffer consisting of 0.5% Triton X-100, 1% universal blocker in phosphate buffered saline and then applied to the sections at 4°C overnight. The standard negative control received the above noted buffer without the

application of primary antibody. Following incubation, all sections were carefully washed with PBS and then incubated in secondary (Invitrogen, A31573 and A21202) fluorescent-conjugated antibodies for 30 minutes. Alexa Fluor conjugated secondary antibodies were used to amplify the positive signal and to visualize the immunoreactivity of the astrocytes (donkey anti-mouse Alexa Fluor 488 [1:200] Invitrogen, A21202), microglia (donkey anti-rabbit Alexa Fluor 647 [1:200] Invitrogen, A31573), and Ferritin (Abcam, ab7332). In order to reduce autofluorescence, sections were incubated in a Cu SO_4 solution (0.01M Ammonium Acetate (Fisher-Scientific, A639-500) and 0.001M Copper (II) Sulfate (Fisher-Scientific, C-495) for 90 minutes, cleared in tap water, and then washed several times in double distilled water. The sections were then mounted with Fluoromount G (Southern Biotech, 0100-01) and coverslipped (Fisher-Scientific, 12-545M).

1.2.5 Microscopy

Images were obtained on an inverted epi-fluorescent microscope (Leica DMI 6000B). The sections were scanned in their entirety at a low magnification and higher magnification images were obtained in the areas with positive iron staining. The areas within the sections were labeled according to a pre-determined grid method. One image was taken of each of the relevant grid sections and compiled to create an output of the entire region.

In order to create an image of the entire tissue of interest for the myelin stain, both the top right hand corners and the bottom left hand corners were set within LAS AF 2.6.3 as the boundaries delineating the size of the tissue section. The computer then took 2x magnification images in a grid pattern encompassing the entire surface area of the tissue. Following which a composite of the image was used to achieve a view of the distribution of the myelin stain within the entire tissue section.

1.2.6 Image Analysis Program

The image analysis program was written in JavaScript. Representative sets of images were chosen from the images obtained from tissues with iron staining. From these photos 3 features of interest (FOI) were manually identified based on the 3 patterns of iron deposition observed. Specifically, iron deposition was found to be differentiated based on both the shade of blue as well as the location within the tissue. The shades of blue were labeled as dark blue, bright blue, and light blue. Similarly, the regions of deposition were identified as: within the neuropil, pericellular, and intracellular. Furthermore dark blue was associated with the intracellular location, bright blue with the pericellular location, and light blue within the neuropil. Images were chosen to include outliers of both directions. Therefore, included in the set of images were cases where the FOI were barely present, cases in which the FOI were observed at a moderate intensity and frequency, as well as cases where the FOI predominated the surface area of the image and at a high intensity. Next, predominant blue hues for each FOI were identified. To determine the specific blue hues associated with each of the 3 FOI the corresponding pixel colors were examined (20-50 pixels depending on the area covered by the feature). As a result up to 4 predominant blue hues were chosen for each FOI, which were called the normative colors.

The analysis engine took as input the images to be analyzed, along with the normative colors of the FOI. Briefly, the analysis engine analyzed every pixel in each image to identify and measure the areas where the normative colors were located, thus identifying and measuring the FOI (in terms of pixels). Finally, information such as the corresponding percentage of the total picture size, and relations between feature sizes were exported in plain textual files for further analysis. All photos obtained from every tissue section were run through the automated program created using the parameters identified and specified above using the representative selection of images.

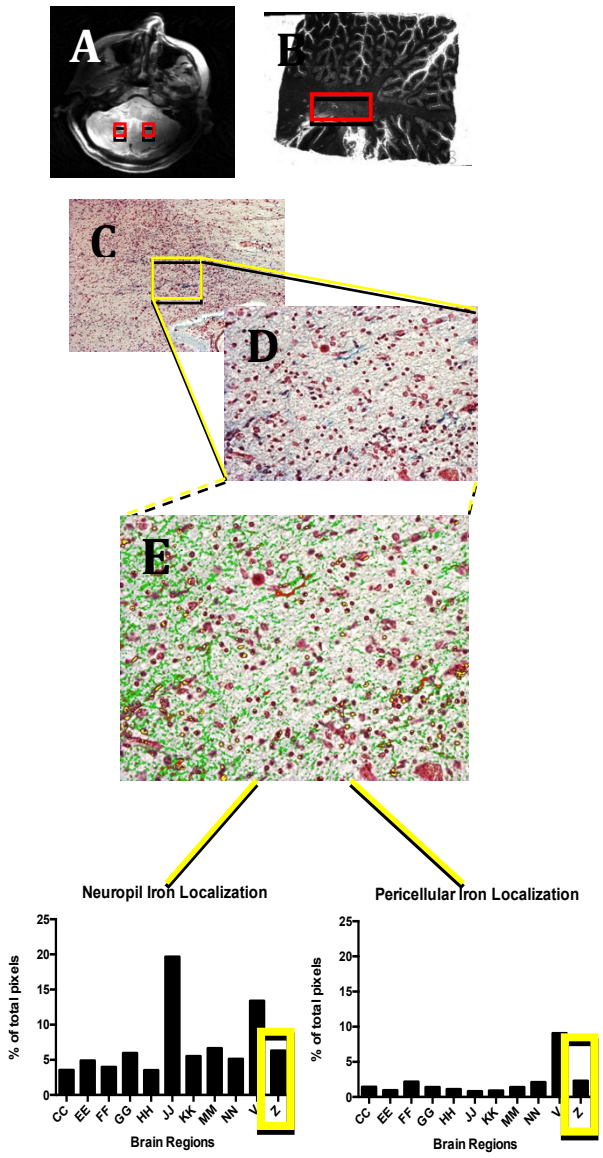

Code was written by Victo Guana. For access to the code please see:

Figure 2-1. A holistic view of the localization and quantification of iron in a specific region within a single patient. A.) MRI image, B.) Myelin Staining using Weil's protocol, C.) & D.) iron staining using Perl's Prussian Protocol, E.) Iron quantification using the Iron Analysis Program, and F.) the visualization of the iron content with respects to the iron content seen in the other brain areas of the patient.

http://victorguana.blogspot.ca/2016/09/identifying-iron-depositions-in.html

1.3 Results

The results of the patients were examined in the workflow order outlined in Figure 2-1. A contiguous patient pool was utilized for the entire work-flow outlined in Figure 2-1. In addition, each section within each Patient was subjected to this work-flow. Maintaining a contiguous patient pool allowed for cross-referencing between MRI images, myelin staining protocols, as well as iron-staining protocols for every brain region in all of the patients. First, MRI images were used to assess iron levels in a region-dependent manner in the pre- and post-mortem patient (A). Next, the tissues of interest (TOI) were sectioned and stained for both myelin (B) and presence of iron (C). Following the staining, the sections stained for iron were run through the Iron Analysis program, in which light blue is depicted by green overlay, bright blue by red overlay, and dark blue by yellow overlay. Together, the bright blue and dark blue staining represent peri-cellular iron deposition, whereas light blue represents neuropil iron deposition. Finally, the quantitative values given by the iron analysis program were graphed with respects to either neuropil or pericellular localization in a region-dependent manner,

To determine whether the myelin stains corroborated the actual presence of a lesion or a plaque, two resources were used. First, the pathology reports were used to positively identify the presence of a lesion or plaque. Secondly, the MRI images were used to make associations between lesions, iron content, and demyelination. Sections that were noted as containing an area of demyelination or plaque by the notes in the pathology reports also showed loss of myelin from the Weil's protocol. Using Weil's protocol, myelin is observed as navy blue and non-myelinated tissue as cream. Loss of myelin was defined as either: an interruption of a blue path (Figure 1A), a cream patch in the middle

of surrounding area of dark blue (Figure 1B), or the extension of cream into areas that should be dark blue (Figure 1C). Using these methods of identification, it was observed that all 52 of the sections from MS patients stained with Weil's Myelin stain corroborated the reported areas of demyelination and plaques in the pathology reports. Specifically, the areas that were identified in the pathology reports as containing lesions were also observed to have corresponding regions of demyelination using Weil's Myelin stain.

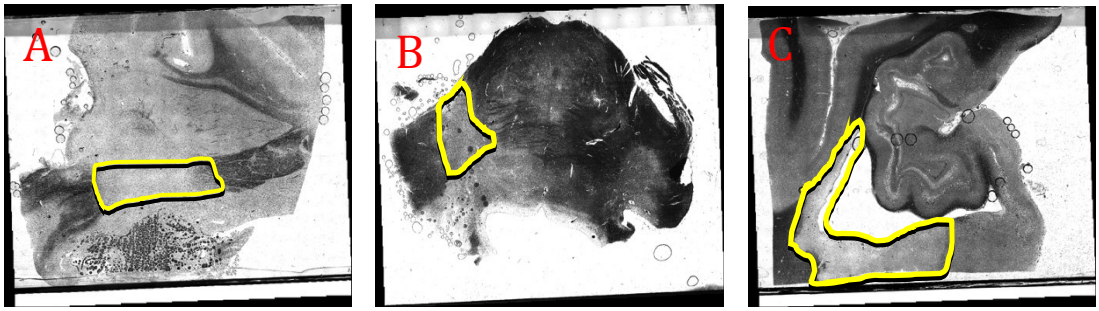

Figure 2-2. Ways in which plaques and areas of demyelination were positively identified using the Weil's Myelin Protocol.

To further analyze the areas of sequential tissue sections were stained for iron. Photomicrographs were obtained of ROI showing positive iron staining (blue). Two patterns of iron staining were observed: peri-cellular and peri-cellular + neuropil. The iron deposition differed between patients as well as within patients between brain areas. Some patients exhibited higher iron staining overall. Within the patients that exhibited clear iron staining, differences between brain regions in intensity of iron and pattern of deposition existed.

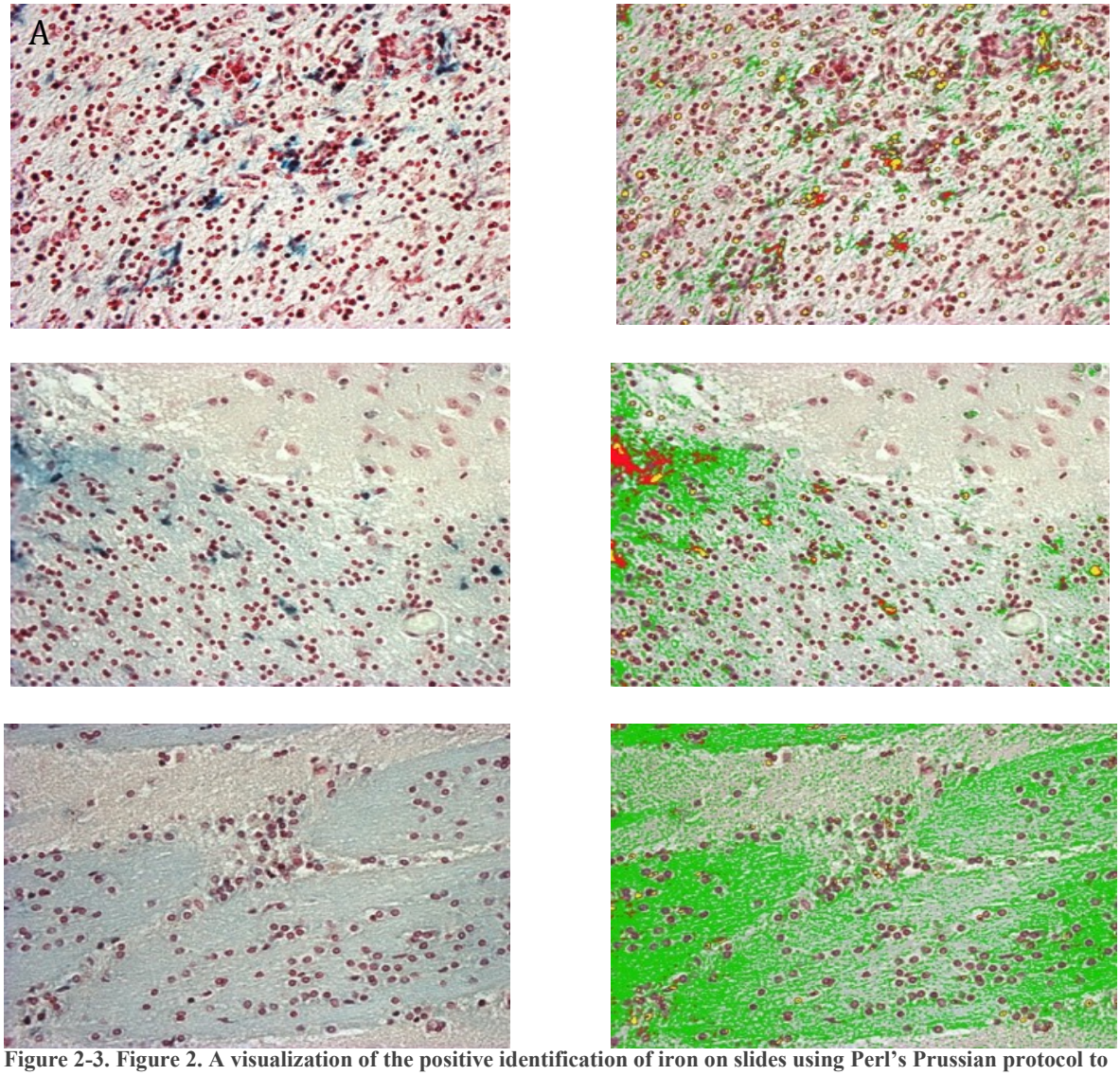

Figure 2-3. Figure 2. A visualization of the positive identification of iron on slides using Perl's Prussian protocol to demarcate areas of iron concentration as blue. Cell bodies are seen as red circles.

Graphs of Iron Localization

To determine whether differences of whole-brain iron deposition patterns existed between patients, as well as within patient iron differences, we plotted the quantitative output measures produced by the image analysis software.

Control Patient

The control patient exhibited high levels of iron staining only in the neuropil locations. Namely, moderate levels in region D (thalamus) and high levels in region E (basal ganglia and caudate nucleus) (Table 2-5). All pericellular areas showed insignificant iron content within the control patient (Figure 2-8).

Table 2-1. The anatomical locations associated to each letter (denoting a particular brain region) in the Control Patient.

Area	Anatomical Location
D	Thalamus
E	Basal ganglia containing the caudate nucleus
F	Putamen and globus pallidus
G	Midbrain including susbstantia nigra and red nucleus
K	Midbrain

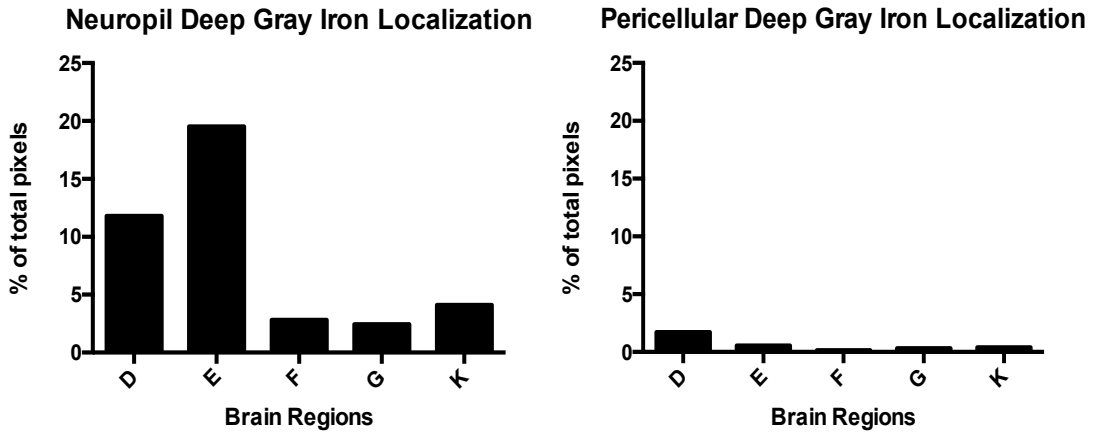

Figure 2-8. The neuropil and pericellular iron localization levels for brain regions examined in the control patient. High levels are identified as value above 15, moderate levels between 10-15, and low levels as below 10.

Patient 1

Patient 1 exhibited variations between neuropil iron and pericellular iron levels were observed (Figure 2-4). High levels of Neuropil iron were observed in brain regions JJ (posterior hippocampus) and V (rostral midbrain) (Table 2-1), whereas moderate pericellular iron levels were observed in V only.

Table 2-2. The anatomical locations associated to each letter (denoting a particular brain region) in Patient 1.

Area	Anatomical Location
CC	Striate polar cortex
EE	Parietal cortex
FF	Hippocampus
GG	Pulvinar
HH	Posterior temporal cortex
JJ	Posterior hippocampus
KK	Mammillary body and basal ganglia
MM	Anterior globus pallidus and putamen
NN	Prefrontal superior frontal gyrus
V	Rostral midbrain
Z	Right dentate nucleus

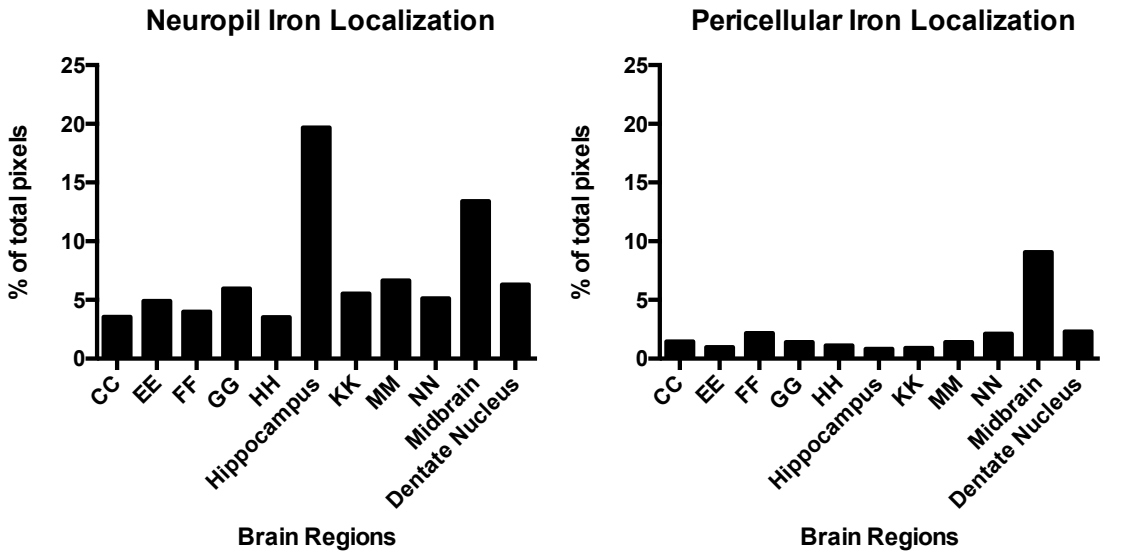

Figure 2-4. The neuropil and pericellular iron localization levels for brain regions examined in Patient 1. High levels are identified as value above 15, moderate levels between 10-15, and low levels as below 10.

Patient 2

Similarly to Patient 1, Patient 2 also exhibited variations between neuropil and pericellular iron levels within brain regions (Figure 2-5). The region that showed high iron levels in the neuropil were regions A (anterior cingulate gyri), G (thalamus), and O (midbrain) (Table 2-2). All corresponding regions were found to have low iron levels in the pericellular locations.

Table 2-3. The anatomical locations associated to each letter (denoting a particular brain region) in Patient 2.

Area	Anatomical Location
A	Anterior cingulate gyri
B	Posterior cingulate gyru
D	Right head of caudate putamen
E	Left head of caudate putamen
G	Thalamus
J	Right posterior cingulate gyrus
K	Left posterior cingulate gyrus
N	Midbrain
O	Midbrain
S	Pons
W	Medulla

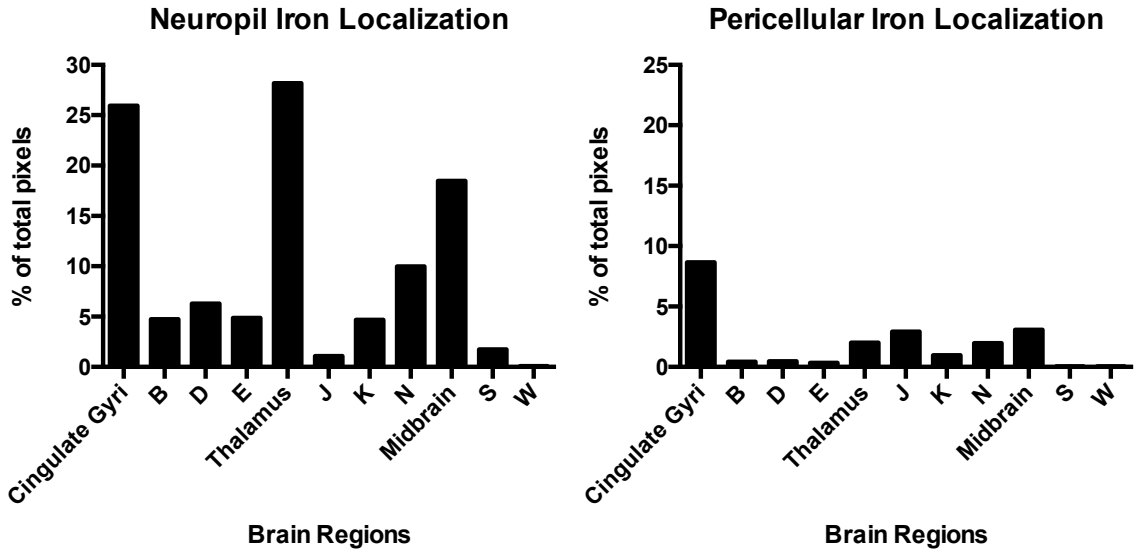

Figure 2-5. The neuropil and pericellular iron localization levels for brain regions examined in Patient 2. High levels are identified as value above 15, moderate levels between 10-15, and low levels as below 10.

Patient 3

Patient 3 exhibited low levels of iron localization in all brain regions, in both neuropil and pericellular locations (Figure 2-6).

Table 2-4. The anatomical locations associated to each letter (denoting a particular brain region) in Patient 3.

Area	Anatomical Location
A	Frontal double watershed zone
B	Left superior hemisphere
C	Left superior hemisphere
E	Left superior hemisphere
F	Right hemisphere
I	Thalamus
J	Occipital lobe
M	Basal ganglia
N	Thalamus with hippocampus
O	Lower midbrain
P	Pons
Q	Pons
T	Cerebellum (with peduncles)
U	Cerebellum

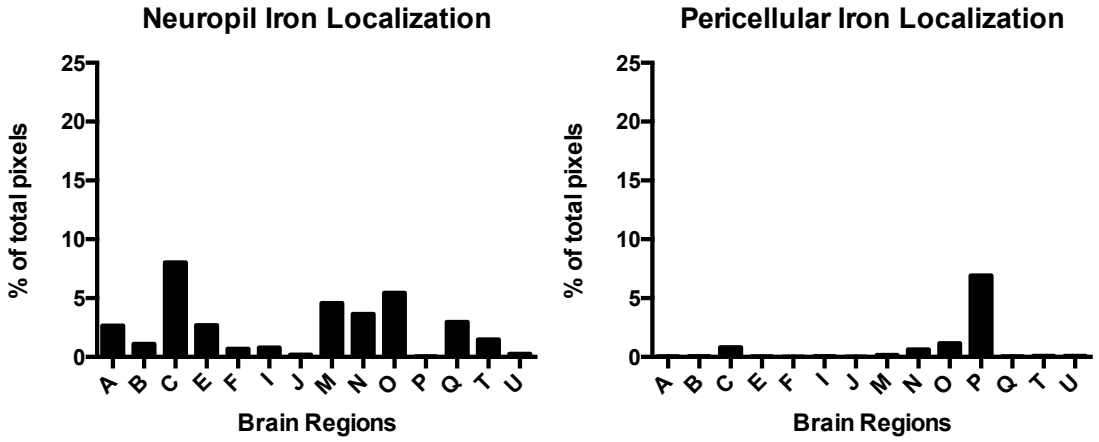

Figure 2-6. The neuropil and pericellular iron localization levels for brain regions examined in Patient 3. High levels are identified as value above 15, moderate levels between 10-15, and low levels as below 10.

Patient 4

Patient 4 exhibited interesting overall trends between neuropil and pericellular iron depositions (Figure 2-7). Negligible iron localization was seen in the pericellular

locations in all brain regions. In contrast, many of the brain regions had moderate neuropil iron localization. Interestingly, region AQ (internal capsule and putamen) (Table 2-4) had high levels of neuropil iron localization.

Table 2-5. The anatomical locations associated to each letter (denoting a particular brain region) in Patient 4.

Area	Anatomical Location
AA	Hippocampus, tail of caudate, lateral ventricle
AB	Corona radiata
AC	Body of the lateral ventricle
AD	Caudate, putamen, globus pallidus
AE	Anterior caudate, putamen, globus pallidus
AF	Right posterior horn of lateral ventricle
AG	Left posterior horn of lateral ventricle
AH	Anterior portion of the third ventricle
AI	Posterior portion of the third ventricle
AJ	Left anterior corpus callosum and cingulate cortex
AK	Right anterior corpus callosum and cingulate cortex
AL	Posterior corona radiata
AM	Hippocampus, tail of caudate
AN	Posterior corpus callosum and cingulate cortex
AO	Right internal capsule and putamen
AQ	Left internal capsule and putamen

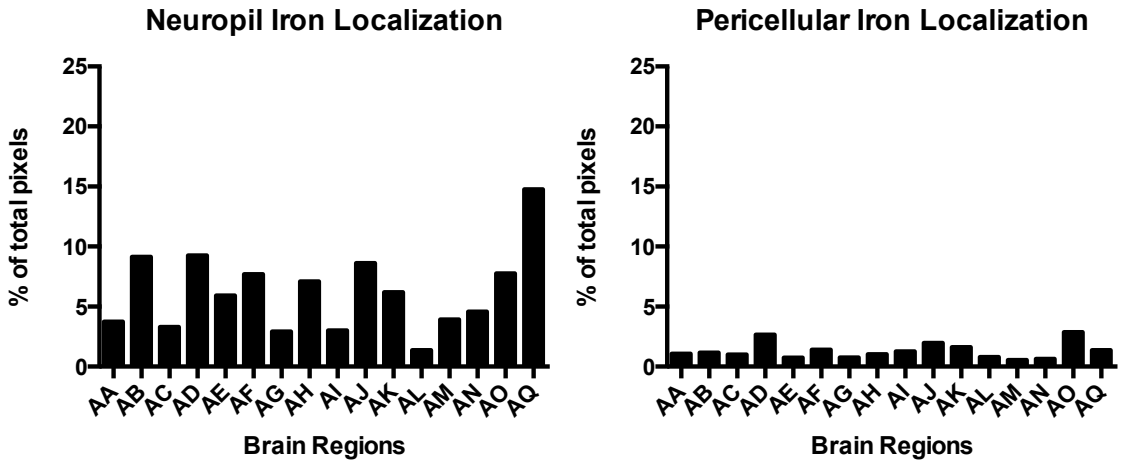

Figure 2-7. The neuropil and pericellular iron localization levels for brain regions examined in Patient 4. High levels are identified as value above 15, moderate levels between 10-15, and low levels as below 10.

Deep Gray Iron Localizations

Due to the reports of increased iron content observed in deep gray areas in healthy patients in the literature, we wanted to more closely look at the iron content in the deep gray areas. Using the iron quantification method outlined in section 1.2.6, we included all areas within each patient that contained regions of deep gray matter.

Patient 1

Patient 1 showed low neuropil iron localization in all deep gray areas, this intensity was similarly matched in the pericellular iron content (Figure 2-9).

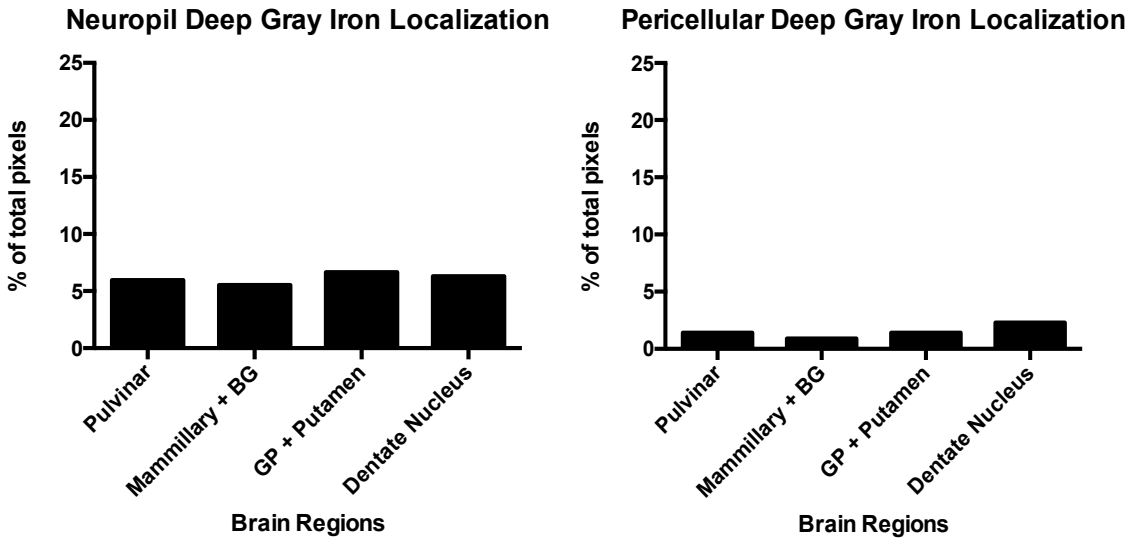

Figure 2-9. The neuropil and pericellular iron localization levels for deep gray brain regions examined in the Patient 1. High levels are identified as value above 15, moderate levels between 10-15, and low levels as below 10.

Patient 2

The thalamus and midbrain showed high levels of neuropil iron accumulation, with moderate associated pericellular levels (Figure 2-10). Conversely, in the corresponding pericellular locations, only low levels of iron localization were observed.

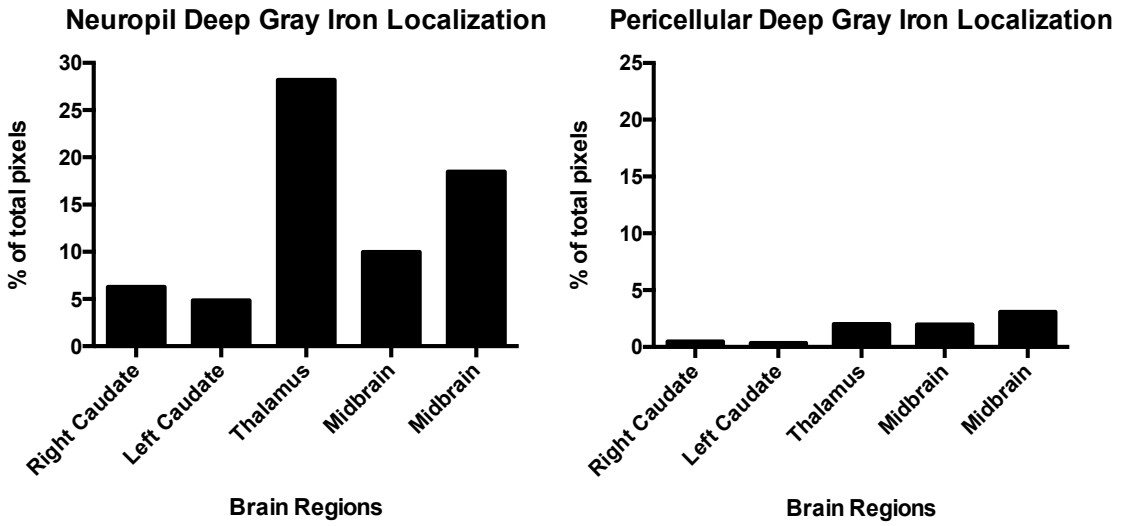

Figure 2-10. The neuropil and pericellular iron localization levels for deep gray brain regions examined in the Patient 2. High levels are identified as value above 15, moderate levels between 10-15, and low levels as below 10.

Patient 3

Patient 3 exhibited low iron levels in both neuropil and pericellular locations for iron localization within all brain regions (Figure 2-11).

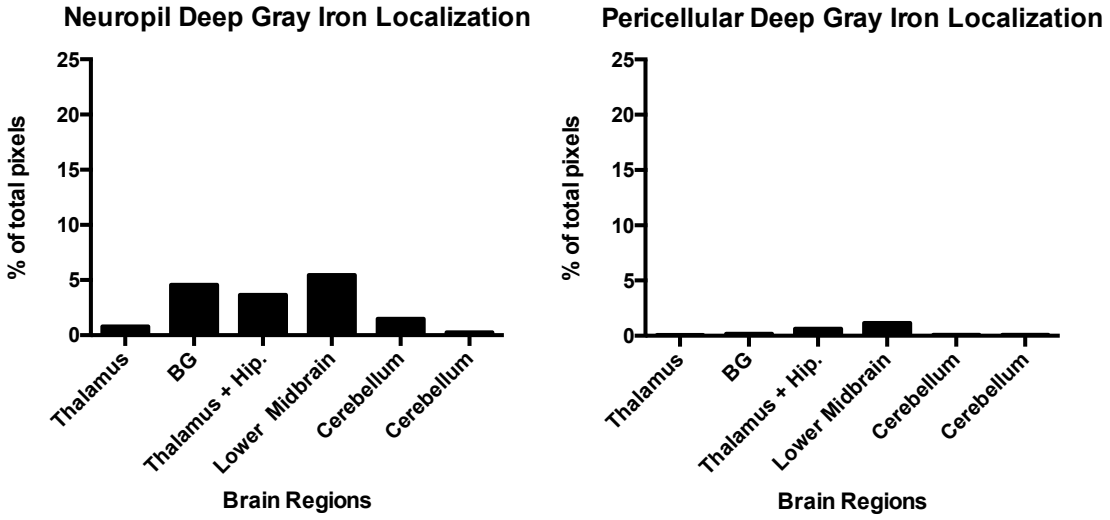

Figure 2-11. The neuropil and pericellular iron localization levels for deep gray brain regions examined in the Patient 3. High levels are identified as value above 15, moderate levels between 10-15, and low levels as below 10.

Patient 4

Moderate iron localization levels were observed in the Caudate + Putamen + GP in the neuropil of Patient 4. In addition, high iron levels were observed in the neuropil in

the internal capsule and putamen (Figure 2-12). All brain regions showed low levels of iron localization in the pericellular locations.

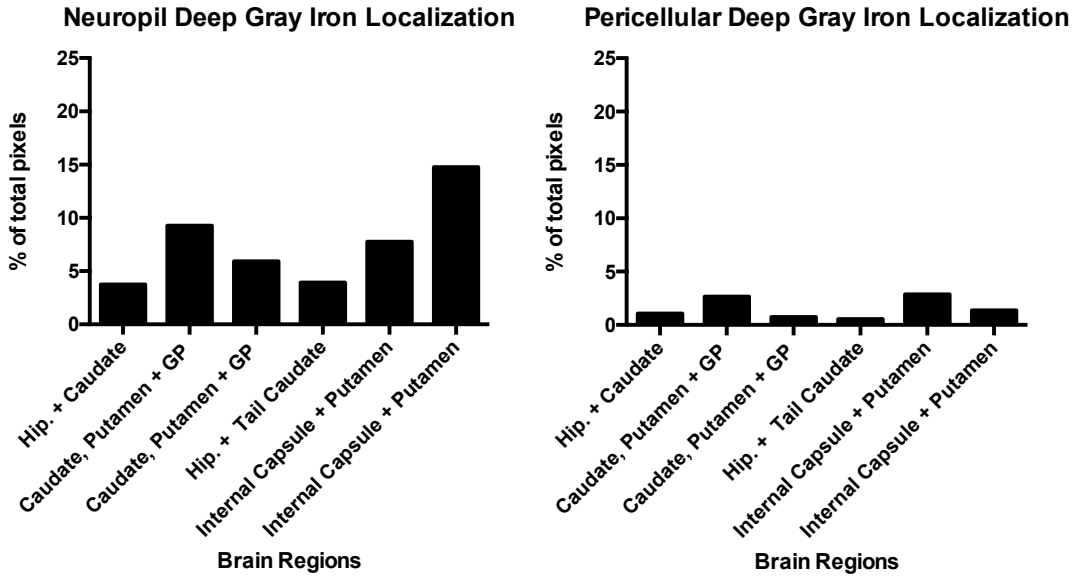

Figure 2-12. The neuropil and pericellular iron localization levels for deep gray brain regions examined in the Patient 4. High levels are identified as value above 15, moderate levels between 10-15, and low levels as below 10.

As previously mentioned, the location of the iron within the specific brain regions is likely to be an important component. This belief underscores the classification of our iron localization into either "neuropil" or "peri-cellular". Iron that is located either in the cell or surrounding the cell membrane ("pericellular") is highly likely to be bound to either iron-storage, or iron-transport proteins. In its bound form iron is unable to participate in chemistry creating ROS. Conversely, iron that is located within the neuropil is more likely to be unbound and therefore available to participate in chemical reactions that create ROS, thereby increasing the inflammation and degeneration in those regions[11,12,14,59,84,87]. With this in mind, we were interested in comparing the locations of the iron depositions/patient with their pathology reports.

Comparison to Pathology Reports

Following the visualization and quantification of the iron load specific to each patient, we then went on the compare the overall iron load as well as region specific iron load to the information presented in the pathology reports. Sections stained for iron and myelin stains were chosen by pathologists, based on the inclusion of a lesion. The sections were excised from the post-mortem brains by the pathologists and paraffin-embedded, following which we received them.

Patient 1 was given a general description regarding his disease progression, which was classified as severe with extensive chronic demyelination. Details were not given on the maturity and/or severity of specific lesions regarding whether they were classified as chronic active, chronic inactive, or acute active lesions. In general Patient 1 exhibited a general baseline of moderate iron localization within the neuropil (Figure 2-4), with certain regions extending into the high levels of iron deposition.

Patient 2 was described as having shadow plaques, which are plaques in the process of remyelination. Within the visualization of the iron accumulation, Patient 2 was observed to have more variation between brain regions (Figure 2-5). A large number of the regions had moderate to high iron load, however the remaining regions had negligible iron load. It is unclear how shadow plaques may correlate with iron load.

Patient 3 was described as having only chronic active and inactive lesions, with no acute active lesions. In comparison to Patients 1 and 2, Patient 3 showed a low iron load, both as a baseline and within regions that exhibited higher levels (Figure 2-6). No regions were found to have high iron levels.

Patient 4 did not have a correlating pathology report.

Patient 5 did not have an accompanying pathology report that specified brain lesions.

1.4 Discussion

The results obtained through the analysis were able to track excess iron deposition in an individual patient, which allowed us to speculate regarding the causality of the iron localization. It was noted that patients differed in their basal iron content. A potential benefit of our iron analysis program is the ability to objectively visualize and eventually establish a baseline of iron deposition levels per patient. Baselines could be created by determining average iron content in non-lesion and non-deep grey regions, thus determining with more specificity what is considered high iron deposition levels in a patient-specific manner.

The data demonstrated high neuropil iron content for some lesions, and moderate to low neuropil iron content for other lesions. We expected to see high neuropil iron content for lesions. However, we did not differentiate between active lesions, inactive lesions, or shadow plaques a priori. It has been noted that inactive or chronic lesions show a lower iron load compared to active lesions. Therefore the disparity in iron load between lesions could be due to the maturity and/or severity of the lesion. Indeed, when comparisons to the pathology reports are considered, a severe disease progression is suggested to be accompanied by high basal iron levels (e.g. Patient 3). This baseline includes brain regions that are not affected by lesions, either chronic or acute. In contrast, a mild disease course characterized by mild neuronal loss and only chronic active and inactive lesions seem to be accompanied by very low basal iron load levels, with few areas containing moderate to high levels (e.g. Patient 1). Comparatively, an MS diagnosis containing numerous shadow plaques as well as mild axonal damage showed a large

variability in the iron load levels (e.g Patient 2). This could be attributed to the various stages of remyelination of the shadow plaques, at the time of death.

This iron quantification suggests that the maturity and/or severity of the lesion plays a part in the iron load contained in and around it. Also, this quantification analysis elucidated the need for a patient specific baseline of iron load. Especially considering that within just five patients we observed vast differences in the baseline of iron-load in the NAWM and unaffected brain areas. Due to the small patient sample, this is an avenue that would require extra information in order to accurately determine.

In addition to the functional differences underlying the iron localization pattern we hypothesize exist in MS, we also found that the technique of quantifying the iron level/brain region was sensitive to identifying various shades of blue. By creating a program that encompassed the entire spectrum of blue shades associated with Perl's Prussian protocol we were able to objectively quantify the degree of iron deposition in a region-specific manner. The use of a program that used a consistent set of shades of blue also created the ability to compare within patient as well as between-patient iron load. Likewise this allowed for the establishment of a baseline that was essential in creating the within- and between-patient comparisons.

1.5 Conclusion

MS research has shown excess iron deposition to be associated with disease progression, as well as with lesions. The use of separate patient pools when conducting human research has limited determination of causality between excess iron deposition, disease progression, as well as disease severity. The results presented in this paper use a

single patient pool and suggest that varying levels of iron load are associated with various aspects of the disease. The baseline iron-load appears to be associated with the severity of the disease, whereas the region-specific iron load looks to be connected to the “maturity” of the lesions in the ROI. The small sample size together with the variation between brain regions/patient made statistical significance an unviable option, therefore further research is required to determine the causality suggested above.

CHAPTER THREE

THE CHARACTERIZATION OF THE TR33B, RAT OLIGODENDROCYTE CELL LINE

Following the observations outlined in the Chapter Two, we were interested in approaching the problem of excess iron deposition in MS from a mechanistic view. It was noteworthy to us that certain areas naturally contain higher iron levels in healthy brains as this speaks to delineation in the brain in which the mechanistic signature of the area requires or leads to excess iron deposition. In order to take the first step in asking and answering a mechanistic question we began with creating a co-culture model. We wanted to create a co-culture model in which the basic cell types and cell interactions seen in the inflammation and demyelination, characteristic of MS, were replicated. Therefore we chose microglia and oligodendrocyte as the cell types to include in our co-culture model.

3.0 Abstract

In cell culture, in order for research to be considered applicable to further medical applications, a wide array of commercially-available animals species to chose cells from, as well as cell types within that species is essential. But there still exist large gaps in the selection of oligodendrocytes within the rat cell lines, which severely limits the questions that can be answered using cell culture techniques. The scientific community has attempted to fill this gap by providing progenitor cells, which produces more unknown variables than the questions they could serve to answer. In this paper, we provide a

characterization of a commercially available rat oligodendrocyte cell line (TR33B) that has previously been poorly characterized and therefore neglected as a viable option to fill this gap. We describe a series of experiments that demonstrate positive oligodendrocyte antigen presentation, as well as projection of myelin within the presence of neurons. We expect increased characterization presented by this paper to increase the usability of these cells within research.

3.1 Introduction

Multiple Sclerosis is a chronic demyelinating disease of the CNS, which is a common topic of current research, as little is understood regarding its aetiology or the mechanisms contributing to disease progression. Much of this current research focuses on understanding the mechanisms underlying both its aetiology, as well as the disease progression. In order to be able to study these avenues of interest cell cultures are often the models of choice. This is due to the fact that cell culture models offer a level of control and mechanistic manipulation that is not afforded by either animal models or post-mortem tissue studies. Therefore, cell culture models allow for a fine-tuning of research questions, particularly those regarding pathological mechanisms. As a result, common cells utilized in such cell culture models are primary and immortalized oligodendrocytes, neurons, and microglia.

Cell culture models are often used in MS research with regards to studying the mechanism affecting demyelination and remyelination, as well as the effect of various pharmacological reagents on the above processes[88–92]. Rats are often the animal model of choice for mimicking various pathologies due to the fact that the brain architecture of rats

is more similar to humans than mice, their physiology is more similar to humans and they are more intelligent than mice[93]. In addition, rat oligodendrocytes have been shown to require less specialized media than do mouse oligodendrocytes and therefore are simpler to culture effectively[94]. However, as far as selection is concerned, there is little available for a rat oligodendrocyte cell line. (Sigma Aldrich, Invitrogen, ATCC, and Charles Rivers) Moreover, the few cell lines that do exist are either poorly characterized, difficult to isolate, are sensitive and thus challenging to obtain high yields from, or are not commercially available. In addition to those obstacles, the commercially available rat oligodendrocyte cell lines often come in the form of progenitor cells (Luis et al., 1992). In this circumstance two options are available: 1.) Neural progenitor cells (NPCs), or 2.) oligodendrocyte progenitor cells (OPCs). In the case of NPCs the cells can differentiate into neurons, astrocytes, or oligodendrocytes, whereas OPCs differentiate into the latter two only. Thus, the immature maturation stage of the cells requires an initial differentiation step followed by an incubation period in which the cells are allowed to reach full maturity, before they can be used in any experiments. The differentiation from progenitor cell into oligodendrocytes can be achieved multiple ways[95–98] including hormonally (T3), physically (shaking), or other growth factors (PDGF)[99–104]. As can be expected, the variety of differentiation methods paired with sparse characterization following them creates uncertainty regarding whether the physiology of the resulting mature oligodendrocytes vary according to the techniques. This point is often overlooked. Such potential disparity, and the lack of research surrounding it creates a possible confound thereby limiting the reproducibility and generalizability of results using these cells.

TR33B Cells

A rat, oligodendroglial cell line - TR33B - was created in 1975[105]. Unfortunately it has remained largely uncharacterized and therefore under underutilized. Sigma Aldrich[106] labels the cell line as "glial", and provides no extra information concerning characterization parameters. The cell line is the result of inducing an oligodendroglioma in the lumbar spinal cord and roots of an inbred Wistar/Furth rat, using *N*-ethyl-*N*-nitrosourea. In the original paper, the morphology is notably described as "cells with many processes"[105]. Equally important is that the characterization of the line was limited at the time to its reactivity to "the common antigen" and the "restricted antigen", both of which refer to unspecified antigens. The common antigen was obtained from antiserum via a series of adsorptions from the liver, spleen, thymus, and kidney and was found to be specific to brain, embryonic tissues, and neural tumors. The restricted antigen refers to an antigen obtained via the same adsorption process, which was found to be specific to the TR33B cell line and two other non-neuronal glial cell lines. Although now seemingly limited, at that time these were novel methods of cell characterization. Nevertheless, with the considerable progress the field of cell research has enjoyed, this description no longer provides adequate data to understand the function and characteristics of these cells in order to be used in modern research.

The aim of this paper is to provide a basic characterization of this poorly described immortalized rat cell line, including cell markers expressed and the production of myelin when in co-culture with neurons. The assumptions underlying this paper are that cell morphology and site of origin provide indicators as to the cell type of the target cell line. Due to the morphology, the region of origin within the CNS, and the reactivity to the common antigen we argue that this cell is an oligodendrocyte cell line.

Furthermore we present evidence depicting a level of characterization that has not yet been provided in regards to the TR33B cell line.

3.2 Methods

3.2.1 TR33B Cell Culture

TR33B cells were obtained from Sigma-Aldrich (Cat no. 8540102)[106]. For use in experiments TR33B cells were first cultured to confluence in T-75 flasks. For use in experiments they were then lifted off using 0.05% trypsin/EDTA and incubated for ~2 minutes at 37°C. Cells were then centrifuged at 300g for 2 minutes, re-suspended, and maintained in F5 (5% FBS) and 200 U/ml penicillin, 200 µg/ml streptomycin in a 37°C, 5% CO2 humidified incubator. The cells were plated at a final concentration of 2 x10^6 cells/m in which density was determined using a cell counter. For transfer experiments 1 mL of re-suspended cells was plated per well in a sterile 12-well plate and incubated at 37°C for 36 h before being treated with the various pharmacological agents or their vehicle control. For all pharmacological treatments the vehicle control was 10 µl of F5 or vehicle solvent per well. The treated cells were incubated for a further 24 h at 37°C.

3.2.2 TR33B Cells + Neurons

Primary rat neurons were used as the source for neurons. Cultures were obtained following the procedure outlined by Dhami et al[107]. The neurons were plated at a density of 2 x 10^5 cells per well. The cultures were maintained with Neurobasal/B27 Media (NBM). 48 h following the plating of the cells 3 µM of cytosine-β-D-arabinanoside (AraC) was added, in order to prevent glial proliferation. AraC treatments were left on the neuronal cultures for 48 h. The cells were refreshed with fresh NBM and allowed to

rest for a further 36 h. All subsequent feedings were done with 1:1 ratio of fresh:conditioned NBM. At 9 DIV $1x10^5$ TR33B's were isolated and added directly into the wells with the neurons. The cells were kept in direct contact with each other for 1 to 3 days. Fixation of the co-culture was done by applying 1 mL of 5% Formalin to each well for 10 m.

3.2.3 Immunofluorescence

2',3'-Cyclic-nucleotide 3'-phosphodiesterase (CNPase)(1:1000), oligodendrocyte lineage transcription factor 2 (Olig2)(1:500), and oligodendrocyte marker O4 (1:500) were used as oligodendrocyte markers for various maturation stages. Glial fibrillary acidic protein (GFAP)(1:1000) was used as an astroctye-specific antibody. Alexa fluor-conjugated secondary antibodies (1:500) were purchased from Invitrogen (A31573 and A21202).

The cells grown in 12-well plates were fixed with 5% paraformaldehyde for 10 minutes, followed by 3 washes with phosphate-buffered saline (PBS). The cells were then blocked with a blocking solution (10% horse serum in PBS with 0.01% Triton) for 1 h. Following further washing, cells were labeled with primary antibodies (in a PBS solution with 0.01%Triton and 1% horse serum) overnight at 4°C. The following day they were washed with PBS and incubated with the relevant fluorescent-conjugated secondary antibody for 2 h under dark conditions. After the final washing step coverslips were applied to the wells using aqueous mounting media containing DAPI stain. The plates were kept covered at 4°C until they were ready to be imaged.

3.2.5 Microscopy

A confocal microscope (Leica TCS SPE Confocal Microscope) was used to obtain photomicrographs of the immuno-labelled direct contact cultures. An epi-fluorescent microscope (Leica DMI 6000B) was used to obtain the photomicrographs of the TR33B characterization experiments.

3.3 Results

3.3.1 Oligodendrocyte Antigen Presentation

To visualize the characterization of the OLGs immunohistochemistry for Olig2, O4, and CNPase .was performed These oligodendrocyte markers were chosen as they label different stages of oligodendrocyte maturity[108]. First, O4 is a marker that is expressed by oligodendrocyte progenitor cells. Second, Olig2 is a pan-oligodendrocyte marker. Third, CNPase is a myelin-associated enzyme that is expressed specifically by mature oligodendrocytes in the CNS. By using markers that are associated with different maturation points we were able to not only positively identify them as oligodendrocytes, but also determine the associated maturation stage.

Table 3-1. A table outlining the various oligodendrocyte markers utilized in the characterization process, as well as their specificity to various maturation stages.

Name of Cell Marker	**Specificity**
O4	Pre-myelinating oligodendrocytes
Olig2	Oligodendrocytes and precursors
CNPase	Myelin-specific, mature oligodendrocytes

The TR33B cells showed positive staining for the oligodendrocyte markers. Specifically, TR33B cells exhibited positive labeling for Olig2 and CNPase, while showing a no labeling for O4 (Figure 3-1).

It was observed that Olig2 staining mildly positively (Figure 3-2), whereas CNPase stained with a high intensity(Figure 3-3). As a result we determined our cultures to be comprised of mature oligodendrocytes with a purity of $\leq$ 92%.

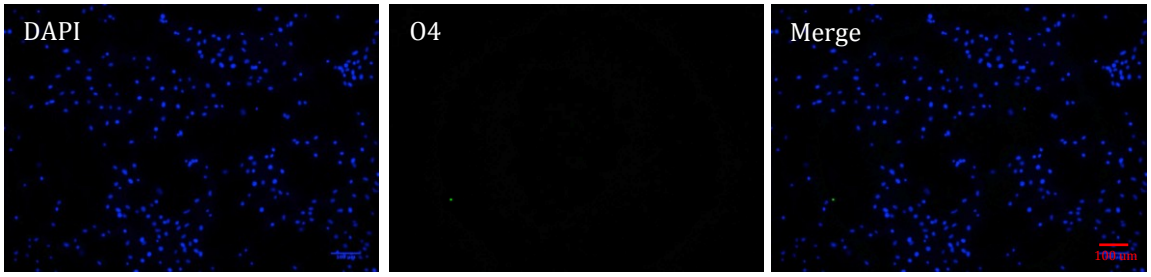

Figure 3-1. Lack of O4 staining seen in TR33B cells. Positive DAPI staining is observed on the far right.

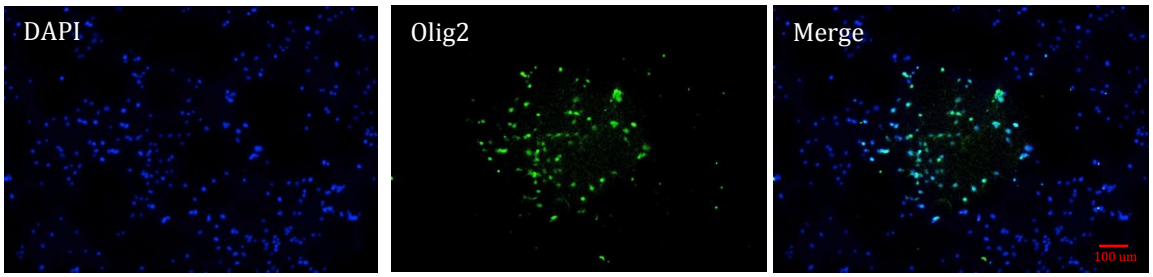

Figure 3-2. Faint positive Olig2 staining observed in the TR33B cells. On the left is DAPI nuclear staining. In the middle is Olig2 staining. The far right image presents the overlap of both the DAPI and Olig2 staining.

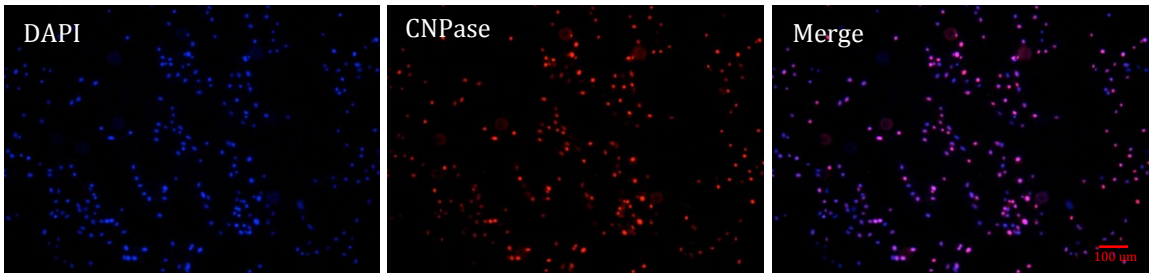

Figure 3-3. Strong positive CNPase labeling of the TR33B cells. On the left is DAPI nuclear staining. In the middle is positive CNPase staining. The right image presents the overlap of the DAPI and CNPase staining.

3.3.2 Extension of Myelinated Processes

Additionally, the TR33B cells were inserted into a direct contact co-culture with primary neurons to observe their myelination abilities. In order to visualize any resulting interactions of the two cells in the co-culture, a neuronal marker (neurofilament) and a myelin-associated-protein (MBP) were utilized. Under these circumstances the markers were used to determine whether the cells possessed the capability of producing myelin in the presence of neurons, and if so, how it was positioned around the neurons. This was an important step as a number of different receptors are required to be both processed and expressed in order to perceive the presence of the neurons and accurately send out myelin to neighbouring axons. In the event the cells demonstrated the ability to extend myelin to neuronal axons, this would suggest that they functionally mimic oligodendrocytes in their cell-cell interactions.

We observed that the cells sent out a MBP positive substance. Minimal MBP-positive staining was observed on Day 1 following the addition of the TR33B cells to the neuronal population (Figure 3-4). When a positive label was seen, it very faint and surrounded only large clusters of neurons (data not shown). By Day 3 there was an

abundance of MBP-positive signal found throughout the co-culture, which enveloped both groups of neurons as well as individual neurons (Figure 3-5 and 3-6).

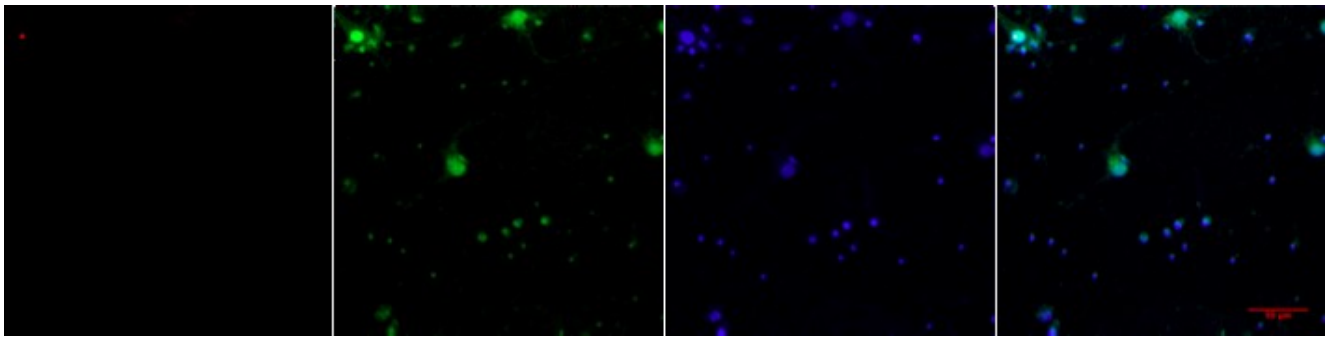

Figure 3-4. Minimal MBP-labeling was observed in 1DIV co-culture of TR33B cells and primary neurons. Negligible positive MBP-labeling (red) was observed following one day of direct contact co-culture with the cortical neurons.

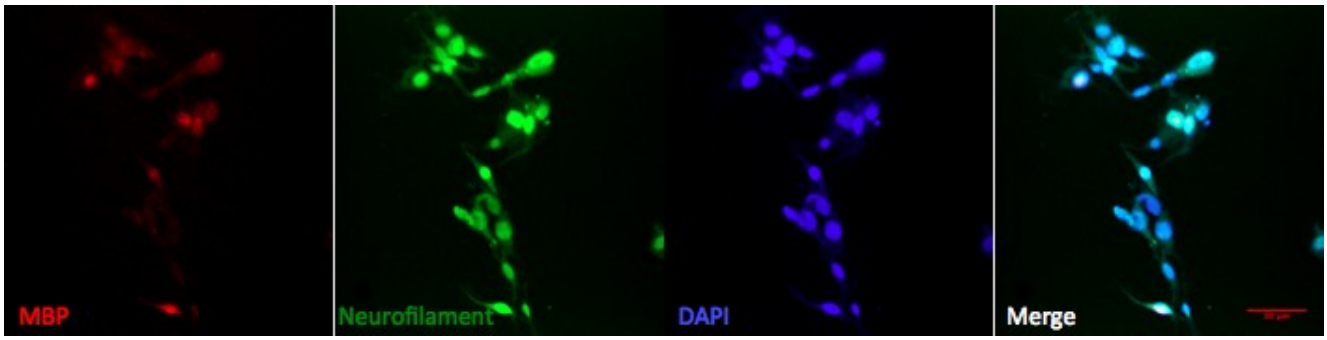

Figure 3-5. Positive MB P labeling observed. 36 hours following the insertion of the TR33B cells into the co-culture model with the neurons positive MBP labeling (red) was observed surrounding individual neurons (green).

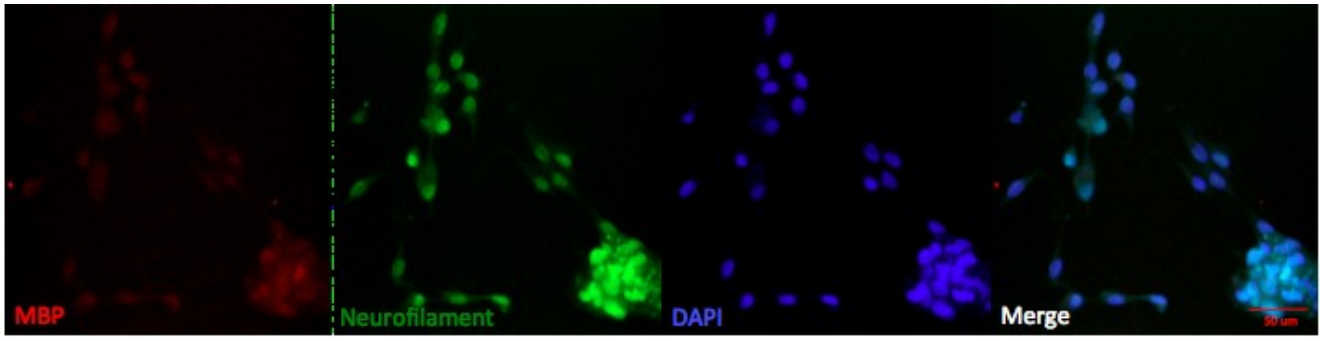

Figure 3-6. Positive MBP labeling observed. In addition to the positive MBP labeling seen above surround individual neurons, cloud-like MBP (red) extensions were also observed surrounding clusters of neurons (green). 36 hours following the insertion of the TR33B cells into the co-culture model with primary neurons.

3.4 Discussion

Our research addresses the lack of characterization of a cell-line and provides a robust, commercially available cell line that has largely gone un-characterized. We established basic characterizations for the TR33B cell line that had not yet been reported. Furthermore, our findings validate the hypothesis that this cell line has characteristics that are similar to an oligodendrocyte cell line. Our results establish positive immunolabeling for antigens that are specific to oligodendrocytes. In addition the morphology of large cell bodies with multiple processes is consistent with oligodendrocyte morphology. When placed in a direct contact co-culture with neurons the TR33B cells produced MBP positive structures, which enveloped both groups of neurons as well as individual neurons. Taking these three major findings together is indicative of a positive characterization of an oligodendrocyte cell line. However, to be positive in this characterization further testing should be done. It could be that this cell line is composed of various cell types. A further possibility is that due to it being an oncogenic cell line

there could be large dysregulations to cell-specific antigens that have yet to be discovered.

Some limitations within our approach were that these cells have a very aggressive growth rate and interaction style with other cells due to their oncogenic nature. This creates a limitation that these cells cannot be handled in ways that primary cells would. Specific attention must be paid to incorporating abnormally low plating densities, low-serum media use, and a rapid rate to establish confluence.

To summarise, our findings indicate that this cell line portrays characteristics consistent with being an oligodendrocyte cell line. These findings demonstrate a new, commercially-available rat cell-line expressing features of oligodendrocytes. These characterizations allows a deeper level of understanding of this cell line than has been previously reported which opens it up to the scientific community as a new option for in-vitro studies.

3.5 Conclusion

The line of rat oligodendrocytes, TR33B, had yet to be fully characterized thereby rendering it an unviable option for cell culture research. We now know that they express antigens of mature oligodendrocytes and have the capability to express myelin basic protein in the presence of neurons. This new level of characterization has demonstrated a rat oligodendrocyte line that is viable for use within experiments. Furthermore, its robust viability and short maturation cycle make it optimal to conduct high throughput experiments.

Further research is required to determine the genetic markers expressed by this cell line such as: immunofluorescence for MOG, and investigation of mRNA for other oligodendrocyte markers such as PLP, Olig1, and Olig2. Furthermore, these cells should be continued being exposed to various co-culture models to observe resulting interactions with other glial and neuronal cells.

Chapter Four

The Synergistic activity of P2X receptors an the HO-1 pathway leads to increased cell death in oligodendrocytes and immunological functioning in microglia

Understanding the mechanisms that play into area-dependent excess iron deposition was the next thing that we were interested in understanding further. This will help us to further understand how these mechanisms can become pathological. Currently, approaches to disease-modifying treatments of MS focus broadly on immune modulation. However, it is likely that, due to the heterogeneity of the iron deposition in the brain, in conjunction with the metabolic differences between these regions, a more targeted approach will be clinically relevant. We feel that understanding which mechanisms underlie the delineation of brain regions expressing excess iron in healthy brains will be the key to us creating effective disease-modifying treatments. Thus, we looked at a pathway that is associated with disease progression in MS as well as a pathway that plays a large role in the metabolism and homeostasis of iron in the brain. We were interested to see whether any synergistic effects existed between these two pathways that could interact with the disease progression of MS

4.0 Abstract

The realm of MS research is focused largely on understanding both the initiating events of the disease as well as the ways normal brain functions become pathological.

Some research in this field is currently interested in the effects of dyregulated iron levels on the aetiology and pathology of MS. Iron is a key component in the physiologically healthy brain, however when it's homeostasis is disrupted it can lead to the induction of ROS-mediated cell toxicity. Significantly, abnormal patterns of iron deposition have been noted in brains affected by MS. In this paper we examine possible cellular mechanisms that may influence the homeostasis and patterns of iron deposition. We describe a set of experiments that manipulate a pathway crucial to iron homeostasis as well as a group of receptors implicated in the disease progression of MS (HO-1 and P2X respectively) to elucidate possible synergistic activity between them. By determining possible synergism we may be able to understand more about how the homeostasis of iron is disrupted in MS, and how it becomes toxic. The results suggest an association between the purinergic receptors and the HO-1 pathway.

4.1 Introduction

Multiple Sclerosis (MS) is a debilitating autoimmune disorder of the Central Nervous System (CNS)[109,110]. In MS the myelin sheath is the target of repeated pathological autoimmune attacks. These attacks lead to demyelination, which is the result of the degradation of the myelin sheath. Although the myelin sheath is produced by oligodendrocytes, the loss of it also confers negative consequences to the neurons it envelops. In particular, this loss leads to a degradation of neural signal transmission, in both speed and fidelity. Cognitive, sensory, and motor deficits are consequently observed, which greatly reduce quality of life[111–113]. Moreover, the cause of demyelination and the full ramifications of it are not yet fully understood[114–116].

Despite the lack of knowledge surrounding the aetiology of MS, some of the malfunctioning brain processes underlying its major symptomatology are understood. For one thing, in the early stages of disease progression cellular dysregulation is observed predominantly in glial cells, whereas neurons become affected as the disease progresses further[117–121]. Glial cells play a vital role in the maintenance of homeostasis in the CNS. They interact with neurons, each other, and incoming signals from the environment, which they then interpret, integrate, and modify. Microglia (MG) and oligodendrocytes (OLG) are types of glial cells, both of which play major roles in MS.

4.1.1 Oligodendrocytes (OLG)

To begin with, a primary role of OLGs is to create the myelin sheath in the CNS. The production of a myelin sheath provides the CNS with high velocity conduction, as well as signal fidelity over time and space[122–124]. The degeneration of oligodendrocytes and their associated myelin sheaths serve as hallmarks of various diseases, including Multiple Sclerosis. The majority of research has focused on the role of OLG as a reactive one. This refers to the common conception that oligodendrocytes primarily respond to the signals sent out by other cells. In contrast, some research has shown that these cells are capable of reacting to external immune challenges in an independent manner rather than merely perpetuating the immune signals expressed by other surrounding glial cells (i.e. microglia and astrocytes). Namely, OLG have been shown to express cytokine receptors and also express members of the JAK/STAT family, which are known to be up regulated in MS lesions. Furthermore, when OLG are stimulated with IFN-γ they have shown to be able to express protective genes against oxidative stress. These findings, coupled with the fact that when mice have OLG that have a suppressed responsiveness to IFN-γ they showed higher OLG apoptosis as well as an increased MS disease progression, suggests

that OLG are able to induce protective mechanisms and potentially even modulate immune responses. Although their repertoire of responses may be more limited than that of MG or astrocytes, it seems increasingly likely that OLG should be viewed as active, rather than passive, concerning immune disruptions within the brain.

4.1.2 Microglia (MG)

MG are the resident macrophages of the brain that act as a link between neurological and immunological functioning. As a result, they assume a ramified state as long as they are under neutral physiology[119], and transform to an activated state in response to an immune violation. In their ramified state they use their long processes to constantly survey the environment, and are involved in maintaining the general homeostasis of the brain. In the case of an immune violation microglia immediately become activated[118,125]. Similar to their ramified state the activated state includes a morphological and functional signature. The morphological signature includes withdrawing their processes and adopting an amoeboid morphology, which allows them to travel to the site of injury. Likewise, their functional signature allows them to respond flexibly to the nature of the injury by encompassing both immune-related roles such as antigen-presentation and cell-cell signalling, as well as maintenance-related roles such as phagocytising dead cells and pathological factors. Chronic activation of microglia has been linked to various neuropathologies including Alzheimers Disease, Parkinson's Disease, Stroke, Traumatic Brain Injury, and Multiple Sclerosis[126].

To add a further layer of complexity to microglia, not only does their activation state determine their functions, but also the method of activation affects the roles they assume, and thus the effect they have in the compromised brain[125,127]. Microglial activation can occur either due to the absence of certain signals (lack of normal

neurotransmitter, decrease in oxygen levels etc.), or the presence of abnormal signals (i.e. bacteria, virus, excessive levels of neurotransmitters etc.)[119,128–131]. Upon activation microglia release a variety of cytokines, reactive oxygen species (ROS), chemokines, growth factors, as well as other toxic molecules. The exact milieu of factors released is determined by the type and strength of activation. One common molecule that is both released from stimulated microglia, as well as microglia responding to in the environment, is adenosine triphosphate (ATP). ATP, in addition to being a major energy source, acts as a chemoattractant to signal the location of the damage to microglia. Moreover, it is the ligand to the family of purinergic receptors[132,132–134].

4.1.3 Purinergic Receptors

The term purinergic receptors denotes a class of molecules that respond to the release of ATP = P2 receptors, or adenosine = P1 receptors. Purinergic receptors have been implicated in various cellular functions including cell proliferation, migration of neural stem cells, apoptosis, and cytokine secretion[132,133,135–137]. P2X receptors are a sub-class of ligand-activated purinergic receptors, with P2X4 receptors being the most widely distributed purinergic receptor in the brain. P2X4 receptors are involved in ATP-mediated cell death as well as activation of the inflammasome, both of which could play an influential role in the disease progression of MS[138–141]. Similarly, P2X7 receptors are found mainly on microglia and play an important role in inflammation and ATP-mediated cell death[137]. Enhanced P2X7 receptor activity is correlated with increased disease progression as well as the peak of neurological symptoms in MS[138–140,142–144]. P2X4 receptors are known to be able to modulate the function of P2X7 receptors[145]. Specifically, P2X4 receptors regulate the release of IL-1β by P2X7 receptors[146], P2X4 plays a role in P2X7-dependent cell death[147], as well as the two receptors exhibiting

reciprocal compensatory expression[145,147–150]. Therefore we hypothesize increased activity of P2X4 receptors may contribute to the disease onset and/or progression of MS.

4.1.4 Iron

Iron plays an important role in normal brain metabolism; it is involved in processes such as myelination and oxidative phosphorylation[151]. Within the physiologically healthy brain the majority of iron is stored as non-heme iron within oligodendrocytes (OLGs) and myelin, within ferritin[123,151]. Ferritin is an intracellular protein that stores iron as well as controls its release. When iron is not associated with a storage or transport protein, it is considered free iron. Free iron, unlike bound iron, can be toxic to the brain. Iron toxicity occurs when the free iron content is higher than the concentration of transferrin available to bind and thereby neutralize the iron. In this free form iron is able to participate in Fenton chemistry, thus producing reactive oxygen species (ROS). In controlled concentrations ROS play an integral role in cell signalling and provide a link to the adaptive immune system. However, in excess concentrations ROS become toxic to the cell[15,46,55,152–154]. Some of the damaging effects induced by excess ROS include: DNA damage, lipid peroxidation, oxidation of amino acids, and deactivating enzymes. Such deleterious effects of unchecked ROS release are implicated in the progression of diseases such as: cancer, Alzheimers Disease, Diabetus Mellitus, Multiple Sclerosis, and even obesity[155].

4.1.5 Iron and Microglia in MS

In a large majority of neuropathologies miroglia are readily activated[46,46,49,50,56,154]. As discussed, microglia can become activated due to a variety of signals, one of which is free iron. Although iron plays a vital role in the homeostasis of the brain, when taken to abnormal conditions, such as excessive uptake or altered

metabolism, it becomes an activator of microglia[117]. Within MS, the highest iron content was found in active lesions, compared to inactive lesions or re-myelinated plaques [46]. Active lesion edges display dystrophic microglia with high iron loads[49,52]. Unlike healthy physiological conditions, in active lesions in MS iron was found to be less associated with oligodendrocytes and more frequently in microglia or the neuropil[52]. Pro- and anti-inflammatory cytokines influence the uptake and release of iron[87]. It is not fully understood whether this excess iron is the cause or result of neuroinflammation and demyelination in MS.

4.1.6 Heme-Oxygenase 1

Heme-oxygenase 1 (HO1) is a member of the Heme-Oxygenase family of enzymes that are essential to the catabolism of heme into carbon monoxide (CO), free iron, and biliverdin[156]. HO-1 is the inducible form of the enzyme and within the CNS it is found within neurons and glial cells. Under "normal" physiological conditions HO confers anti-inflammatory and immune-modulatory properties[154,156]. Upon up-regulation HO-1 and its products appear to have a bi-phasic effect, with normal levels prompting cyto-protection and excessive production invoking cellular injury [157–159]. The trophic and toxic effects from this molecule appear to be environment dependent. It is possible that both the toxic and trophic effects of HO-1 can be concordant within the same brain. It is suggested that the intensity of HO-1 induction, and therefore also its toxicity, is determined by the chemistry of the local micro-environment.

Given the above points, the biphasic effect of HO-1 makes deciphering its role within the disease progression of MS difficult[46]. Within the pathological conditions of MS and EAE, an induction of HO-1 has been linked to the formation of plaques, increasing inflammation, as well as the progression of the disease [160–162]. Our interest in

the role it may play in MS is due to accumulating research concerning the participation of excess iron in the disease pathology of MS.

Based on the equivocal role HO-1 may play, a possible method of determining its relevance to MS is through understanding possible interactions/interdependence on other molecules implicated in MS pathology and disease progression. One such avenue of interest is to examine interactions between purinergic receptors and the HO-1 pathway. Purinergic receptors (such as P2X7) are known activators of MG, and also up regulated in MS[138–140,142,143,163]. If interdependence between the two pathways exists, it follows that the synergistic activity of these two receptor types may affect the pathological progression of MS.

To determine whether any impact of synergistic activity between the two signalling pathways could influence the detrimental effects observed against oligodendrocytes in an inflammatory disease such as MS, a co-culture model was created to mimic these settings. In order to accurately mimic the conditions experienced *in situ* in the brain, pro-inflammatory pre-treatments were applied to the microglial cultures after which they were inserted into the co-culture with oligodendrocytes. This was then used as an environment in which to observe the effects various pharmacological reagents had on the activation state of the microglia, and consequently the viability of the associated oligodendrocyte pool.

4.1.10 Biological Activity of the Pharmacological Reagents

Agonists and antagonists for both the signalling pathway of HO-1 and P2X receptors were chosen in order to pharmacologically tune the target pathways up and down. By tuning their activation levels independently and in tandem we were able to determine whether synergistic effects exist. Positive identification of synergistic activity

would occur when the effect of the single drug treatment was altered by the additional application of the second drug treatment. In this case if the tandem application were to increase pro-inflammatory cytokine release levels as well as signals of cell death respective to the single application, the synergistic activity would be considered potentiating in nature. Similarly, the reverse would suggest an inhibitory synergistic activity.

Table 4-1. A table depicting the roles the various pharmacological manipulators have on the two target pathways.

Pharmacological Reagent	**Effect**
SnPP	Antagonizes HO-1 pathway
Hemin	Agonizes HO-1 pathway
CORM-2	Antagonizes P2X receptors
ATP	Agonizes P2X receptors

Hemin - is an iron-containing molecule, which is used in cell culture conditions to pharmacologically increase the activity of the HO-1 receptor. The increased activity releases free iron into the environment and thusly behaves in a pro-inflammatory manner by increasing levels of iron-derived ROS[164–166].

Tin Protoporphyrin (SnPP) – is a heme analogue that selectively inhibits HO-1. It is commonly used to study the role of HO-1 in both cells and animals[156,167,168].

ATP – Within the confines of these experiments ATP was used in a two-fold manner. First it was utilized as pro-inflammatory pre-treatment to mimic the environment of neuroinflammation in the co-culture. Secondly, it was used as a pharmacological agonist for the purinergic family of receptors[132,133,141].

CORM-2 (tricarbonyldichlororuthenium (II) dimer) is a carbon monoxide-releasing molecule[169]. The use of CORM-2 within these experiments was twofold. First, CORM-2 is a specific and effective antagonist for the P2X4 receptor[170,171]. Secondly, due to its function of releasing CO (which is a by-product of the HO-1 pathway) it possesses the ability to create a feedback-loop and thus influence the activity level of the HO-1 pathway. By combining tandem drug treatments with the dual role CORM-2 may perform, we have 2 ways of investigating possible synergistic activity of the two target systems.

The following cell types were used to create a model representing the basic

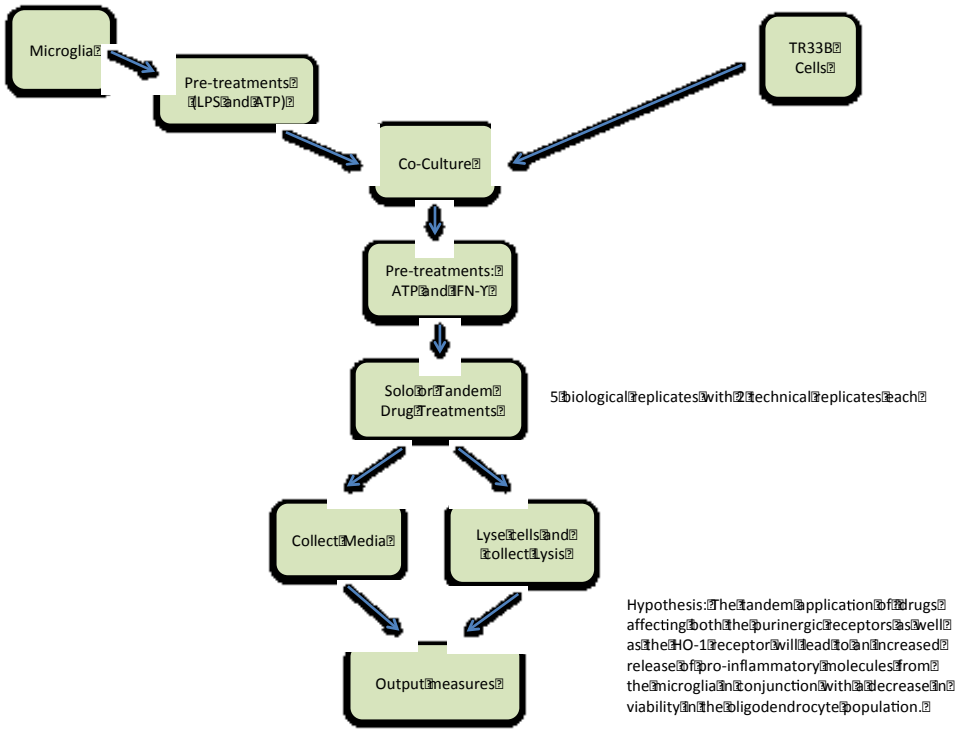

Figure 4-1. The experimental outline followed using the co-culture model.

pathological cell interactions characterized by MS. First, primary rat microglia were used to model the inflammatory contribution to CNS injury in MS. Second, TR33B cells (an oligodendrocyte line derived from an oligodendroglioma) were used to represent the

oligodendrocyte population. The main effect measured was that of HO-1 and P2X modulation on microglia-mediated oligodendrocyte injury. The effect of purinergic receptor activation was examined as a potential role in the bi-phasic activation model of HO-1. Mechanistic experiments were additionally performed to determine the expression and secretion of cytokines by microglia and oligodendrocytes within the co-culture model. Outcomes of this research could contribute to the development of novel pharmaceutical approaches targeting the source and propagation of inflammation within the neuroinflammatory environment of MS.

4.2 Materials and Methods

4.2.1 Materials/Reagents

Adenosine triphosphate (ATP), Interferon gamma (IFN-γ), Hemin, tin protoporphyrin (SnPP), and were obtained from Sigma-Aldrich. All other materials unless otherwise specified were obtained from Thermo-Fisher Scientific. An automated cell counter (Millipore, Scepter Cell Counter) was used for determining cell density. A cell plate reader (Molecular Devices MD5) was used for measuring colorimetric and fluorescent assays including cell viability and fluorescence in ELISA experiments. Fluorescent digital microscopy images were obtained using the inverted microscope (Leica DMI6000B and Leica TCS SPE Confocal Microscope) to visualize cell populations and their respective morphology.

4.2.5 Primary Microglial Cell Cultures

All animal procedures were carried out in accordance with the guidelines of the University of Alberta Animal Care Committee. Microglia were isolated from mixed glial cultures at 14–21 days in vitro (d.i.v.) as previously described[172,173]. Breifly, whole brains were dissected from postnatal day one Sprague–Dawley rat pups, the meninges removed, and cells dissociated by trypsinization and trituration. Mixed glial cultures were grown in T-75 flasks coated with poly-L-lysine and maintained in F10 and 200 U/ml penicillin, 200 µg/ml streptomycin in a 37°C, 5% CO2 humidified incubator. Upon reaching confluence, and for the use in experiments, microglia were isolated from T-75 flasks and the density was assessed using an electronic cell counter. Isolation of microglia from the mixed glial culture was performed using Lidocaine (15mM). Following the addition of Lidocaine, the cells were incubated for 15 minutes at 37°C and shaken at 100 rpm. Cells were then centrifuged at 300g for 2 minutes and re-suspended in F1 media twice, for a final concentration of $1x10^{5}$ cells/mL. Isolated cultures were maintained in F1 and 200 U/ml penicillin, 200 µg/ml streptomycin for the duration of the experiment. Microglia isolated from at least 5 different litters of pups were used.

4.2.6 TR33B Cells

TR33B cells were obtained from Sigma-Aldrich (Cat no. 8540102). For all experiments TR33B cells were used between passages 5 to 20. A single passage was delineated by the cells reaching and maintaining confluence for 3 days, following which they were lifted off using 0.05% trypsin/EDTA and re-plated in a fresh T-75 flask at a density of ~ 1 x 10^5 cells/ml.

For use in experiments TR33B cells were first harvested from T-75 flasks and density was determined using a cell counter. Cells were lifted off using 0.05% trypsin/EDTA and incubated for ~2 minutes at 37°C. Cells were then centrifuged at 300g

for 2 minutes, re-suspended, and plated to a final concentration of 2 x10^6 cells/ml. They were maintained in 5% FBS (F5) and 200 U/ml penicillin, 200 µg/ml streptomycin in a 37°C, 5% CO2 humidified incubator. TR33B cells from at least 5 different aliquots were thawed and cultured independently of each other.

4.2.7 Co-Culture Model

For use in the co-culture model primary microglial cells were isolated as outlined in section 2.4.1 and plated on hanging 0.4µm polystyrene 12-well inserts at a concentration of 1 x10^5 cells/ml. Microglia cells were kept in an incubator for 24 h following which priming pharmacological agents (ATP, and IFN-y) were applied (1mM, and 0.1ug/mL with 0.01%BSA respectively) for 24 h. The well inserts containing the primed microglia were then removed and placed immediately into 12-well plates containing the confluent layer of TR33B cells (as outlined in section 4.2.6) (Figure 4-2). At this point, the various pharmacological agonists and antagonists for the HO-1 and P2X receptors were applied in various combinations and allowed to incubate for a further 24 h.

The co-culture was maintained in a F2.5 media. For all pharmacological manipulations equal volumes of F2.5 and either dH20, PBS, or DMSO were used as the vehicle controls. Following the different pharmacological manipulations and incubation periods, cell supernatants and lysates were collected and cell viability was assessed.

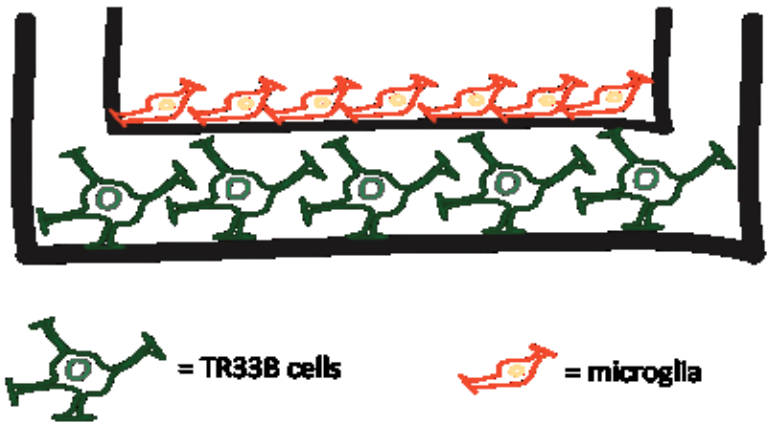

Figure 4-2. A schematic representation of the co-culture model used for the experiments. As depicted, the TR33B cells were grown in a confluent layer at the bottom of a well. The microglia were grown in a well insert, and added at specified time-points.

4.2.8 Pharmacological Treatments

Different classes of agonists and antagonists of the P2X4 receptor and the HO-1 pathways were studied. These pharmacological manipulations were applied at varying dosages based on previously determined effectiveness and pharmacology (ex. IC50).

In order to evaluate the ability of an inflammatory trigger to control the number and activation of target receptors on microglia cell surfaces over time, microglia were challenged with IFN-γ or ATP for 12 h. The specific drug concentrations were chosen based on their ability to change the number of target receptors in microglia *in vitro*, manipulation of which could control oligodendrocyte viability. The microglia were subjected to 6 different conditions (Table 1). Condition A was the control condition in which the cells were not stimulated with either any pre-treatments or any following drug treatments. Condition B included the pre-treatments only, namely a 12 h incubation period with either IFN-γ or ATP. Continuing with pre-treatments were Condition C and

Condition D, which also included a subsequent incubation time with either single drug applications or tandem drug applications, respectively.

Table 4-2. An overview of the various treatments applied to the co-culture model. All pre-treatments were applied to the microglia population prior to their insertion into the co-culture model. All tandem and single drug treatments were applied to the co-culture model.

Treatments
A.) Control – no pharmacological manipulation
B.) Pre-treatment (IFN or ATP for 12 h)
C.) Pre-treatment (12 h) + **Single** Drug Treatment (12 h) -C2, ATP, Hemin, and SnPP
D.) Pre-treamtent (12 h) + **Tandem** Drug Treatment (12 h) - C2 + SnPP, C2 + Hemin, ATP + SnPP, ATP + Hemin
E.) Single Drug Treatment (**no pre-treatments**) (12 h) - C2, ATP, Hemin, and SnPP
F.) Tandem Drug Treatment (**no pre-treatments**) (12 h) - C2 + SnPP, C2 + Hemin, ATP + SnPP, ATP + Hemin

Finally, both Conditions E and F involved only single and tandem drug applications for a 12 h incubation period with no pre-treatments. All six conditions were applied to the co-culture model. In order to closely mimic the cellular signatures observed under inflammatory conditions the pre-treatments were applied to the microglial cultures prior to their insertion into the co-culture model. Following the pre-treatments the microglia were then transferred into the co-culture model where the single and tandem drug applications were then applied to both the MG and the TR33B simultaneously. Similarly, in Conditions E and F where no pre-treatment was applied the microglia were transferred to the co-culture model 12 h prior to the single and tandem drug applications. Following the final incubation period viability, cytokine, enzyme, and protein assays were conducted on the TR33B cells and media.

4.2.9 TNF and IL-1β ELISA

TNF and IL-1 β were measured from the media of the co-culture model. Although OLG express receptors for both IL-1 β and TNF, they have not been shown to secrete these cytokines[174]. Therefore, the levels measured originated from the microglial cells of the co-culture model. The concentration of TNF and IL-1β were all measured by sandwich ELISA. The capture antibodies were diluted to their working concentrations (TNF -720 µg/mL, IL-1β - 144 µg/ml), 100 µl/well was added to a 96 -well plate and left to incubate at 4°C overnight. Following the incubation, the capture antibody solution was removed and the wells were coated with a blocking solution (phosphate buffered solution (PBS) with 1% bovine serum albumins (BSA)) to block nonspecific antigen binding for 2 h at room temperature. Following the removal of the blocking solution, 100 µl/well of standards (TNF- 160 ng/mL, IL-1β - 220 ng/ml) and samples were added and allowed to incubate for 2 h at room temperature. A biotinylated goat anti-rat secondary antibody was applied following washing and aspirating the plate, this antibody was incubated for 2 h at room temperature. Fluorescence was developed by adding 100 µl/well of 20mM Amplex Red (excitation 530 nm and emission 590 nm). The fluorescent response was measured on a microplate reader. Protein concentrations were determined by linear regression.

4.2.10 HO-1 ELISA

HO-1 was measured from the media of the co-culture model. The sandwich ELISA procedure determined the presence and concentration of the enzyme HO-1 in the co-culture media. The assay procedure outlined by the provider was followed (Enzo Life Sciences, ADI EKS 810A). Briefly, the 96-well polystyrene plate was coated with the capture antibody at a concentration of 480 µg/ml. 100 µl of HO-1 standards (stock of 5 µg/ml) and samples were added to the appropriate wells. The standards and samples were

allowed to incubate for 12 h at 4°C. Following the incubation period the plate was aspirated and washed 3 times. 100µl/well of HO-1 detection antibody (stock solution 18 ng/µl) was then added to all of the wells and allowed to incubate for 1h at room temperature. The plate underwent the wash/aspiration cycle again. The conjugate antibody was added (100µl/well, stock solution 50 ng/µl) and allowed to incubate for 0.5 h at room temperature. Fluorescence was developed by adding 100 µl/well of 20mM Amplex Red (excitation 530 nm and emission 590 nm). The fluorescent response was measured on a microplate reader. HO-1 concentration was determined by linear regression.

4.2.11 Cleaved Caspase-3 ELISA

Similarly, the expression levels of cleaved caspase-3 were detected using a sandwich ELISA kit (R&D systems, DYC835-5). The assay procedure outlined by the provider was followed. Specifically, expression levels of CC3 were measured directly from the cell lysate of the oligodendrocyte pool. First, the capture antibody was diluted to a concentration of 2.0ug/ml in PBS and 100 µl was added to each well of a 96-well polystyrene plate and incubated at room temperature overnight. Following the incubation period the plate was aspirated and washed 3 times with Wash Buffer (0.05% Tween 20 in PBS). Next the 300 µl of Blocking Buffer (1% BSA, 0.05%NaN_3 in PBS) was added to each well for 1 h at room temperature. The aspiration and wash step was repeated. Subsequently the standards and samples were added to the appropriate wells and allowed to incubate for 2 hours at room temperature. Following another round of aspiration and washing the Detection Antibody was diluted to a concentration of 150 ng/ml and 100 µl was added to each well. After an incubation period of 2 hours at room temperature the

plate underwent the wash/aspiration cycle again. Streptavidin-HRP was then added to each well (100µl/well, 1:200 in PBS) and allowed to incubate for 0.5 h at room temperature. Fluorescence was developed by adding 100 µl/well of 20mM Amplex Red (excitation 530 nm and emission 590 nm). The fluorescent response was measured on a microplate reader. CC3 protein concentration was determined by linear regression.

4.2.12 Statistical Analysis

Parametric statistical analyses were used under the assumption that the cell populations being used were normally distributed and had homogeneous variance. A one-way analysis of variance (ANOVA) was performed on the results of the viability and cytokine measurements. Sidak's Multiple Comparisons Test was used to further specify any significant differences seen on the from the one-way ANOVA test with a p-value of ≤ 0.05.

4.3 Results

Cells were pre-treated with either IFN-γ or ATP. These molecules were specifically chosen based on their involvement in the innate immune system as well as initiating an inflammatory response in physiological conditions. ATP is a damage associated molecular pattern (DAMP) molecule. IFN-γ is the main immune-modulatory cytokine released by the binding of pathogen associated molecular patterns (PAMPs) to the TLR receptors (which are the primary PAMP receptors). Using two different types of immune activators is particularly relevant when concerning MS, as the aetiology remains unknown. Hypotheses surrounding its aetiology include environmental, immunological,

genetic, and infectious factors. Therefore the use of MG activators that encompass different aspects of the hypotheses makes such experiments relevant to the nature of MS.

4.3.1 Single Drug Treatments

The co-culture model released little to no TNF and IL-1β into the media under control conditions as well as with pre-treatment with ATP. However, both TNF and IL-1β were released upon pre-treatment with IFN-γ. Conversely, HO-1 was released under all conditions. Although HO-1 was released under control conditions the pattern of release differed from that seen with ATP and IFN-γ pre-treatments. The difference in release observed in HO-1 suggests that ATP affects the HO-1 pathway in preferential way compared to the release profiles seen in TNF and IL-1β (Figure 4-3).

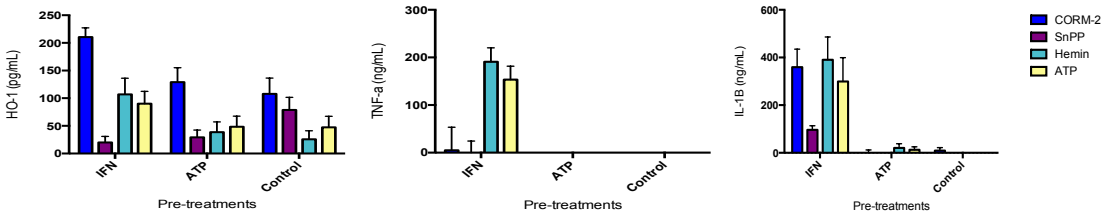

Figure 4-3. The release levels of HO-1, TNF, and IL-1β in response to single drug treatments. The microglia were pre-treated with either ATP or IFN-γ, following which the single drugs were applied to the co-culture. Data displayed are mean +/- SEM of 5 experiments. P < 0.05

Based on the data presented in Figure 4-3, we can observe that both TNF and IL-1B present with negligible release levels in the presence of ATP pre-treatment. Therefore, all data described in the following sections regarding comparisons between HO-1, TNF, and IL-1B will be referring to the IFN-y pre-treatment groups unless otherwise specified.

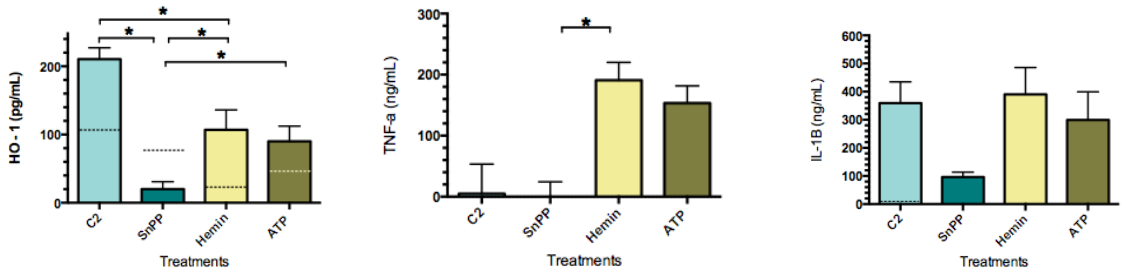

Figure 4-4. A more specific look at the single drug treatments. Only the IFN-γ pre-treatment groups are presented in order to clearly observe significant differences between release levels. The dotted lines represent the level of release for each molecule in the co-culture model without any pre-treatment applied. Data displayed are mean +/- SEM of 5 experiments. P < 0.05

4.3.2 Tandem Drug Treatments

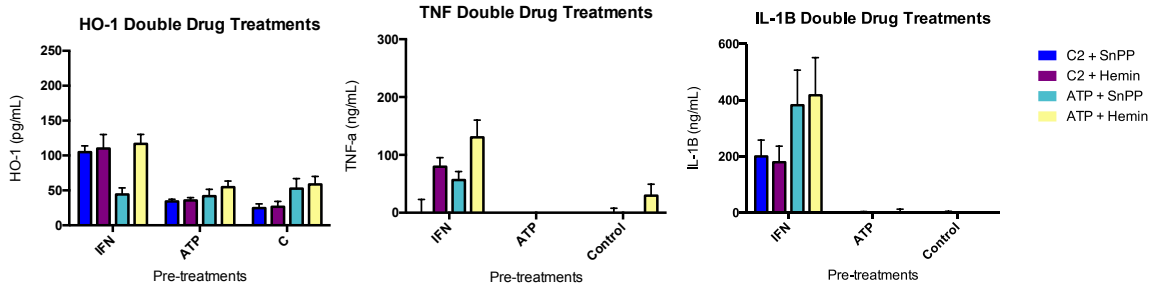

Figure 4-5. The release levels of HO-1, TNF, and IL-1β in response to tandem drug treatments. Data displayed are mean +/- SEM of 5 experiments. P < 0.05

To further investigate the different release profiles between TNF, IL-1β, and HO-1 tandem drug treatments were conducted. When comparing the single to the tandem drug treatments a possible association in activity is seen to occur between the HO-1 and the purinergic pathways (Figure 4-3 and 4-5). The application of the P2X inhibitor, CORM-2, leads to a lifting of the inhibitory effects of the HO-1 antagonist, SnPP, on the HO-1 pathway. Agonizing the HO-1 receptor with the application of Hemin leads to high levels of both TNF and IL-1β, which can only be significantly reduced in IL-1β with the addition of CORM-2, a pattern that is mirrored in TNF. Antagonizing the HO-1 pathway with SnPP leads to low release levels of both TNF and IL-1β. This is attenuated in IL-1B with the application of CORM-2 (P2X antagonist). Interestingly, a similar trend towards relieving the decreased release profile in TNF is observed, however with the addition of the P2X agonist ATP.

4.3.3 CORM-2 Cytokine Results

By treating the co-culture model with the application of CORM-2 either alone or in tandem with Hemin or SnPP we observed a significant decrease in HO-1 release in both tandem applications groups (Figure 4-6). Similarly, this was reflected in IL-1β release with the application of Hemin to CORM-2 decreasing the release levels. In contrast, TNF showed a different trend, with little to no release being observed with the initial application of C2 only and then the application of Hemin to C2 increasing TNF release (not significant).

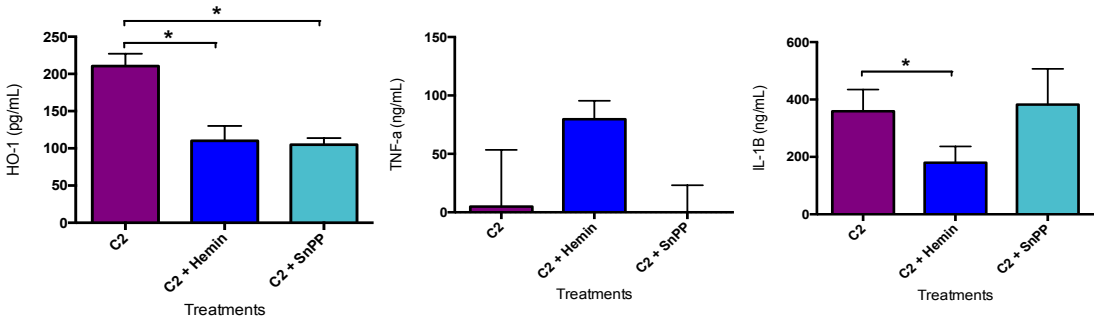

Figure 4-6. A focused presentation of CORM-2 (purinergic antagonist) and the agonist and antagonist of the HO-1 pathway. Data displayed are mean +/- SEM of 5 experiments. P < 0.05

4.3.4 CORM-2 CC3 Results

Neither the single nor tandem drug treatments seemed to significantly affect the levels of CC3 release. Although no significant differences were observed between the various treatments with CORM-2, it is interesting to note that the application of CORM-2, either alone or in tandem, increased levels equally in the ATP pre-treatment group (Figure 4-7). The IFN-γ pre-treatment group exhibited little CC3 release in any of the CORM-2 conditions.

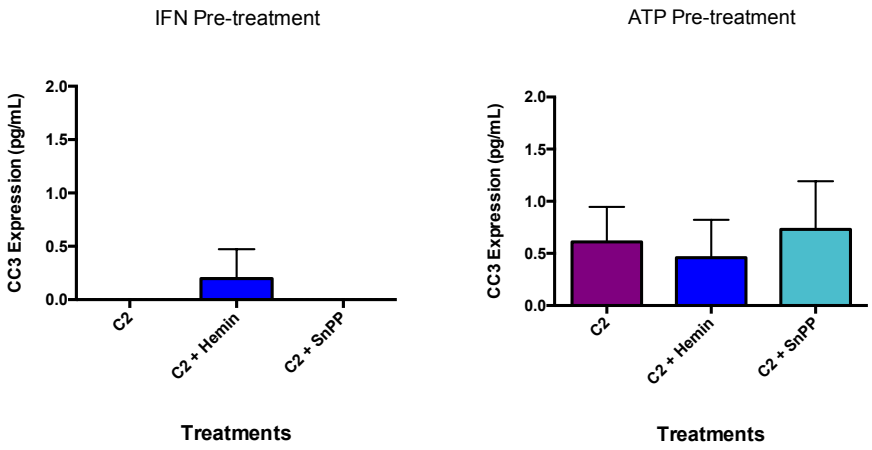

Figure 4-7. A focused view of the expression levels of CC3 from the interaction of CORM-2 (purinergic antagonist) and the agonist and antagonist of the HO-1 pathway. Data displayed are mean +/- SEM of 5 experiments. P < 0.05

4.3.5 ATP Cytokine Results

Significant differences in release profiles were observed only with the addition of SnPP to ATP in TNF specifically (Figure 4-8). In this condition levels of released TNF decreased significantly compared to what was released with the application of ATP alone. Additionally, this trend of the addition of SnPP to ATP decreasing release levels was mirrored in HO-1 data.

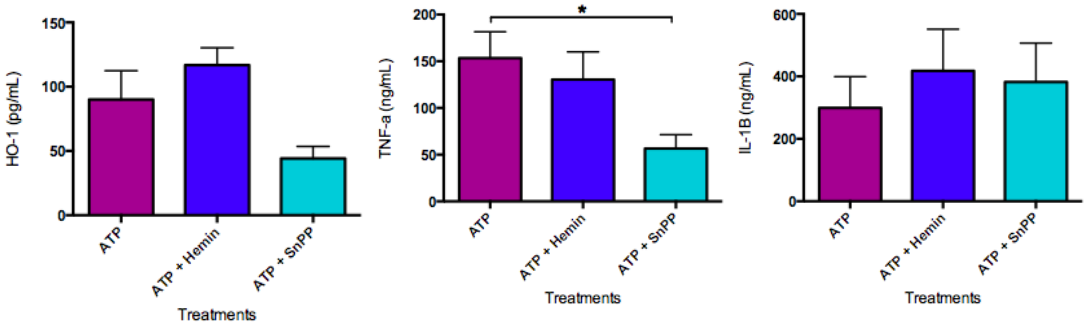

Figure 4-8. A focused presentation of ATP (purinergic agonist) and the agonist and antagonist of the HO-1 pathway. Data displayed are mean +/- SEM of 5 experiments. P < 0.05

4.3.6 ATP CC3 Results

An increase in CC3 release was observed in the ATP pre-treatment groups, specifically with the addition of the HO-1 agonist Hemin (Figure 4-9). Following a similar trend as observed in the C2 drug treatments, IFN-γ pre-treatment did not produce

any noteworthy CC3 release levels, whereas in the ATP pre-treatment the simultaneous application of ATP and Hemin produced increased expression levels. Important to note is that a similar trend was observed between these results and those obtained from the Hemin and ATP pre-treatment results. Namely, that neither of the two agonists alone elicited large expression levels of CC3, but when applied in conjunction they produced the highest levels observed overall.

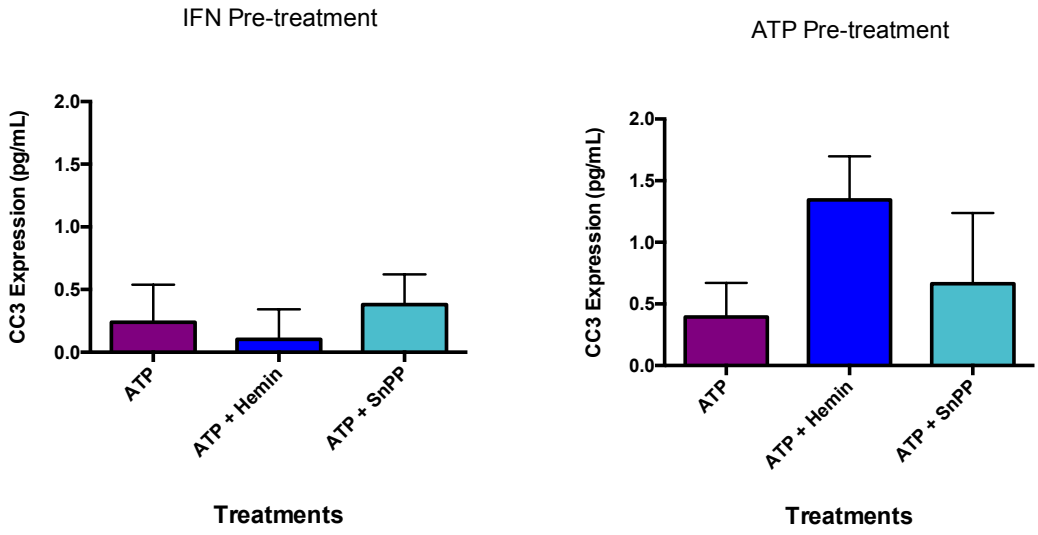

Figure 4-9. A focused view of the expression levels of CC3 from the interaction of ATP (purinergic agonist) and the agonist and antagonist of the HO-1 pathway. Data displayed are mean +/- SEM of 5 experiments. P < 0.05

4.3.7 Hemin Cytokine Results

Similarly to the ATP result, only one significant difference was observed, namely a decrease in the release profile of IL-1β with the addition of CORM-2 to Hemin (Figure 4-10). Whereas the trends in TNF suggest a difference in reaction to Hemin + C2 in a decrease is observed. Interestingly, HO-1 release levels stayed constant across all Hemin conditions.

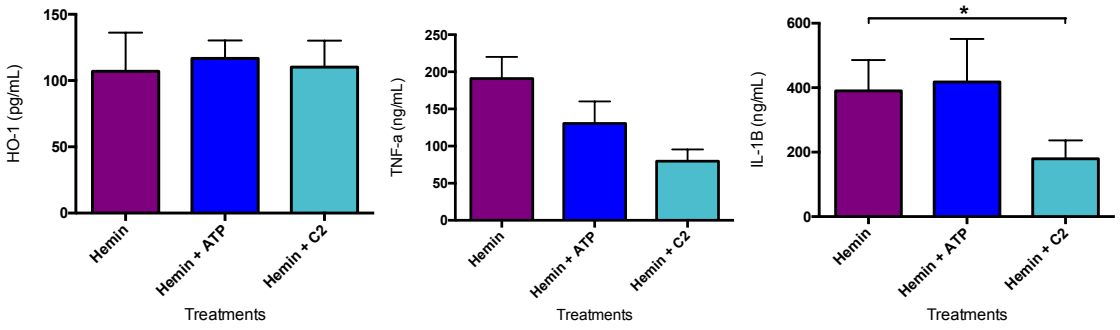

Figure 4-10. A focused presentation of Hemin (HO-1 agonist) and the agonist and antagonist of the purinergic receptors. Data displayed are mean +/- SEM of 5 experiments. P < 0.05

4.3.8 Hemin CC3 Results

Cells were shown to express increased levels of CC3 in response to the tandem application of Hemin and ATP, however only in the ATP pre-treatment group (Figure 4-11). Similarly to other results, IFN-γ pre-treatment showed a negligible increase in CC3 release.

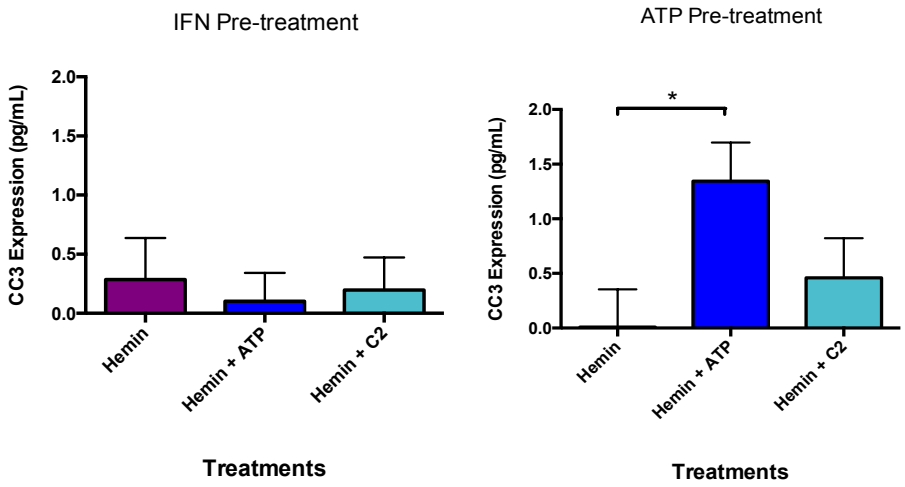

Figure 4-11. A focused view of the expression levels of CC3 from the interaction of Hemin (HO-1 agonist) and the agonist and antagonist of the purinergic receptors. Data displayed are mean +/- SEM of 5 experiments. P < 0.05

4.3.9 Tin Protoporphyrin Cytokine Results

Similarly to the CORM-2 result, we observed a large increase in the release of both HO-1 and TNF with the tandem application addition of SnPP and ATP compared to single SnPP application (Figure 4-12).

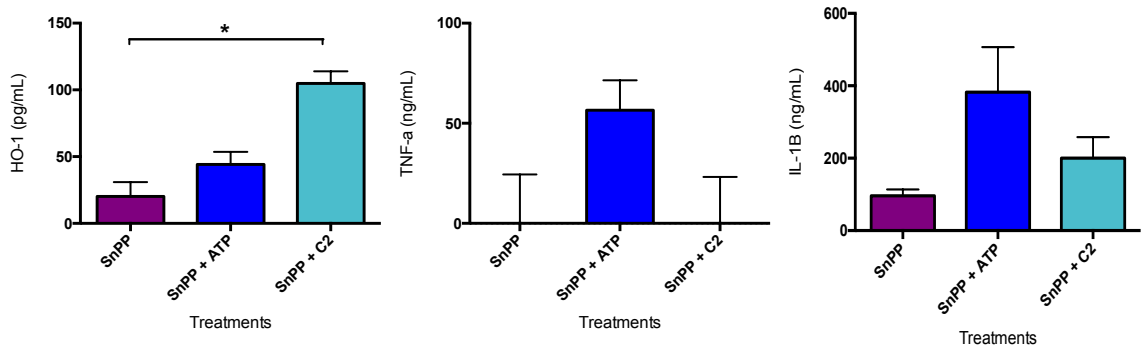

Figure 4-12. A focused presentation of SnPP (HO-1 antagonist) and the agonist and antagonist of the purinergic receptors. Data displayed are mean +/- SEM of 5 experiments. P < 0.05

The greatest synergistic activities were observed with the tandem application of pharmacological agents that affect both the HO-1 and P2X receptors. Specifically, the tandem application of the HO-1 receptor antagonist SnPP and the P2X receptor agonist increased the release of pro-inflammatory cytokines. Conversely the tandem application of both the HO-1 antagonist SnPP and the P2X antagonist C2 significantly increased release of HO-1. This suggests that the pathways are correlated in the directionality of their effects in the simulated inflammatory environment regarding HO-1 levels. Furthermore, they appear to be opposed in their directionality in regards to the release of pro-inflammatory cytokines. Specifically, that the simultaneous inhibition of the HO-1 pathway with the stimulation of the P2X pathway increases release of pro-inflammatory cytokines. Whereas the tandem inhibition of both the HO-1 and P2X pathways leads to an increase in the anti-inflammatory enzyme HO-1.

4.3.10 SnPP CC3 Results

Similarly to the CORM-2 results, no noteworthy changes in CC3 release levels were observed in either the single or tandem SnPP application groups (Figure 4-13).

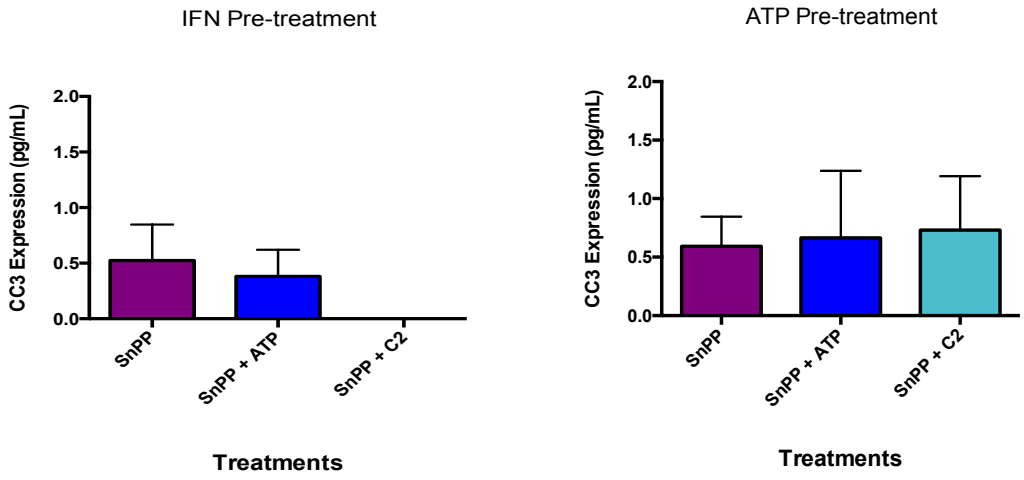

Figure 4-13. A focused view of the expression levels of CC3 from the interaction of SnPP (HO-1 antagonist) and the agonist and antagonist of the purinergic receptors. Data displayed are mean +/- SEM of 5 experiments. P < 0.05

4.3.6 Cleaved Caspase-3 Expression Results

Contrary to the results observed in the cytokine release profiles, increased CC3 expression was observed in the tandem drug treatments in response to ATP pre-treatment compared to IFN-γ pre-treatment (Figure 4-14).

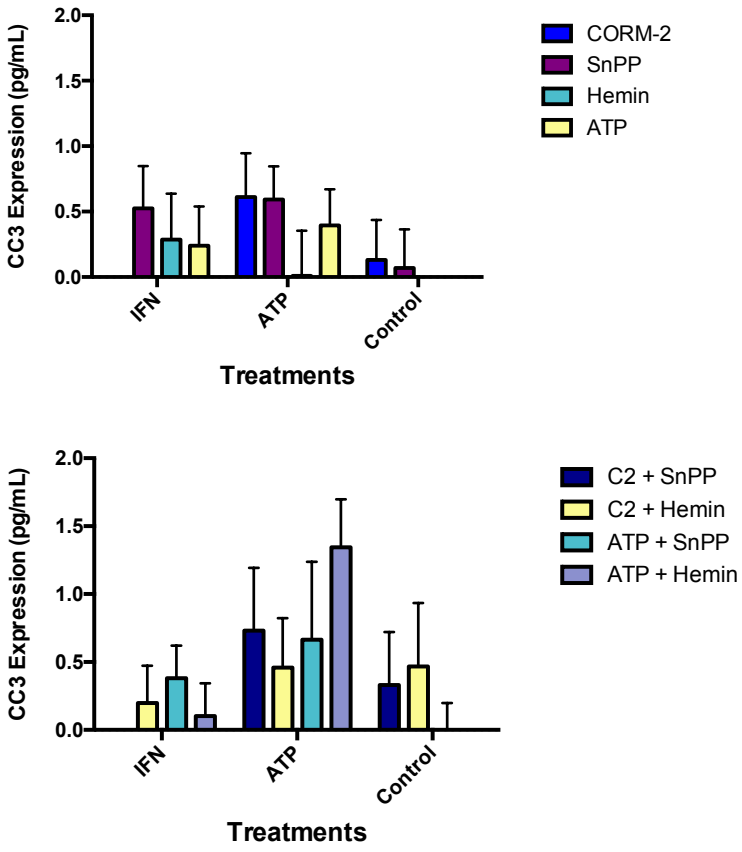

Figure 4-14. The expression levels of CC3 in response to the single and tandem drug treatments. The cells were pre-treated with either ATP or IFN-γ, following which the single drugs were applied. Data displayed are mean +/- SEM of 5 experiments. P < 0.05

In addition, a difference in CC3 expression profile was also observed between ATP and IFN-γ pre-treatment groups in both single and tandem applications of pharmaceuticals.

4.3.11 ATP + Hemin CC3 Comparison

Of the findings obtained by the CC3 ELISA the more significant were observed in the Hemin + ATP group with ATP pre-treatment. As was noted in all other results, negligible expression differences were observed in the IFN-γ pre-treatment group (Figure 4-15).

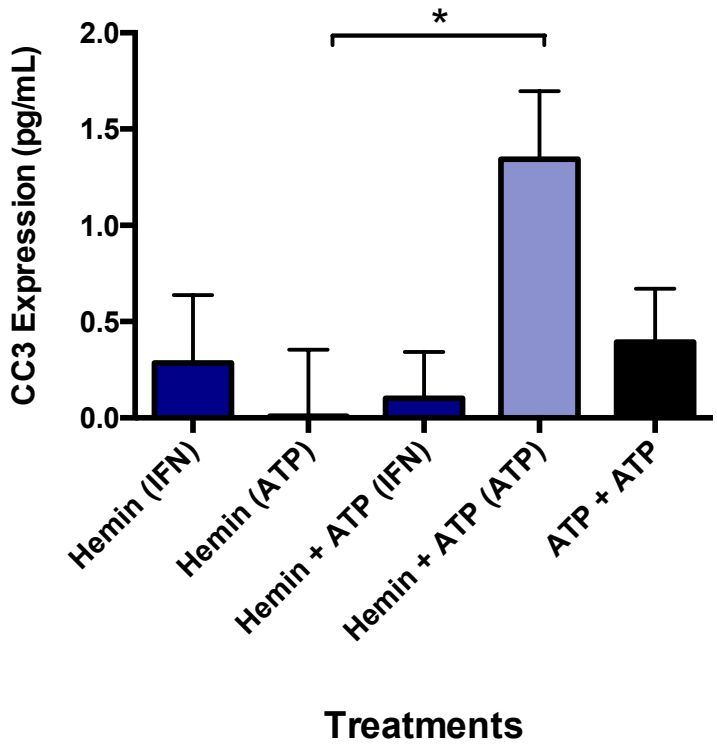

Figure 4-15. A focused view of the resulting CC3 expression level observed between different temporal applications of Hemin and ATP. Both single and tandem applications are shown above, with both pre-treatment conditions. Data displayed are mean +/- SEM of 5 experiments. P < 0.05

The CC3 expression levels mirrored the trend that was observed in the TNF release profiles specifically in the CORM-2 and Hemin groups with IFN-γ pre-treatments. Additionally, the ATP pre-treatment groups exhibited higher levels of CC3 expression than seen in the IFN-γ pre-treatment groups Of further interest is that both the TNF and IL-1β ELISAs were run on media samples whereas the CC3 ELISA was run on lysate samples. The maintenance of the trends over two such different measures further strengthens the corroborative quality of the CC3 results.

As previously mentioned, it was observed that the release profile of CC3 differed between IFN-γ and ATP pre-treatment. The difference lay within the overall quantity of activation, but also in how the certain drug combinations that provoked increased release levels changed based on the pre-treatment conditions. That is to say that the tandem

application of both agonists as well as both antagonists increased CC3 release levels in ATP pre-treatments group but not in the IFN-γ pre-treatment group.

4.4 Discussion

The release levels of each cytokine in response to the single drug applications were used to compare the tandem drug applications to, which was used to help guide our interpretation of our data. By using this as our baseline we controlled for the differences in release profiles between each group of drug applications.

CORM-2 is the antagonist of the P2X receptor family, and antagonists of this type are known to inhibit the pro-apoptotic and pro-inflammatory functions conferred by these receptors. Therefore, it was interesting that this inhibition lead to an increase in both IL-1β and HO-1 levels, as IL-1B is largely viewed as a pro-inflammatory cytokine. Consequently we hypothesize this to be the case because in acute injury (as mimicked by the pre-treatment with IFN-γ and ATP) CORM-2 may play a dual role. First, it acts as an antagonist for the P2X receptors. Second, by releasing CO, which is also a metabolite of the HO-1 pathway, it is hypothesized it could activate feedback loop, thereby indirectly increasing HO-1 pathway activity. This is further supported by the observation that the co-application of both the HO-1 and P2X agonists produced high levels of 1L-1B, HO-1, TNF, as well as CC3. Given these points, it seems that simultaneously co-agonizing the HO-1 and P2X pathways leads to increased cell death.

As previously described, the pre-treatment drugs were chosen based on their inclusion into either the DAMP or PAMP family of molecules. Specifically, ATP was chosen for its role as a DAMP, and IFN-γ due to the fact that it is the main immune-

modulatory cytokine released upon the binding of PAMPs to their receptors. Specifically when addressing hypotheses regarding mechanisms underlying MS, activators of various natures are important as the aetiology is not only poorly understood, but also hypothesized to be multifaceted in its contributing factors. By using both a PAMP and an associated molecule of the DAMP pathway we are modeling some of the various factors that are thought to contribute to the aetiology of MS. Our results are indicative of DAMPs priming MG towards a pro-apoptosis mode (stimulate pathways that lead to a toxic outcome). Whereas PAMPs tune the MG to an increased immune awareness and function, therefore producing a higher cytokine release profile. Thus we suggest that MG are more likely to reduce the viability of oligodendrocytes when in the presence of DAMPS, and more likely to adopt an immune-mediating function when stimulated by PAMPs.

Within an immune-aware environment it seems that HO-1, as well as the combined efforts of both the HO-1 and the P2X pathways, predispose microglia towards cell signalling due to the cytokine release profiles observed. Specifically, agonizing the HO-1 pathway increased the release of both TNF and IL-1β, while antagonizing it had the reverse effect. Another point of interest is that the inhibition of both the P2X pathway through the application of CORM-2 and the HO-1 pathway through the application of SnPP, increased release levels of HO-1. This suggests that the inhibition of the P2X receptor affects the inhibitory effect of the HO-1 pathway. This interesting ability of CORM-2 to inhibit the inhibitory effect of SnPP could be tied to its role as CO-donor, which may allow it to interact in a potentiating manner with the HO-1 pathway. This further corroborates some of the data that suggests HO-1 can take on a deleterious role

under certain conditions. Our results suggest that the nature of provocations experienced by the immune system largely impacts the switch to a deleterious role. In response to provocation from DAMPs, as represented by ATP, HO-1 appears to adopt a pro-inflammatory role.

The most compelling evidence of the synergistic activity of the two pathways is seen in the CC3 expression level differences based on altered temporal applications of ATP and Hemin. Significantly, when the two are applied temporally separated (ATP pre-treatment followed by Hemin application) there is negligible CC3 expression. In contrast, following simultaneous application of Hemin and ATP the highest expression of CC3 was observed. Notably, this effect is only observed within the ATP pre-treatment condition, as it was absent in both the IFN pre-treatment condition and control condition. This suggests that the two pathways may interact in a variety of ways depending on the environment. Specifically, the difference in cell death and activation based on temporal application suggests that these pathways have a synergistic activity that is correlated in the directionality of their results when stimulated with ATP.

Furthermore, these results corroborate previous data suggesting that HO-1 can adopt an injurious function[175–178]. Namely, HO-1 seems to act in a protective manner in situations that mimic acute injury and an injurious manner in conditions that mimic chronic injury. The initial application of ATP followed by Hemin mimics the environment surrounding a cell when an initial insult and its subsequent resolution is followed by activation of the HO-1 pathways. In this condition the result is no cell death. The simultaneous application of ATP and Hemin mimics a chronic environment in which there is no resolution of the initiating event, and the continuous injury coincides with

HO-1 release. In the case of the chronic injury large amounts of cell death are subsequently observed. Overall temporal activation of the two pathways with respects to the initial injury seems to be the determining factor in whether HO-1 plays a beneficial or harmful role towards oligodendrocyte viability.

This work corroborates the findings that under dysregulated conditions HO-1 can switch from a protective to a toxic role[157–159]. Furthermore, the data has shown that this switch is greatly dependent on the types and strengths of the signals present in the microenvironment.

4.5 Conclusion

The HO-1 pathway and the purinergic receptors may have associations between their mechanisms in pathological circumstances. Specifically they are similar in their directionality of effect when facing CNS perturbations. This possible association appears to be multi-faceted depending on the type of perturbation faced. When the perturbation is pathogenic in nature the results are increased cytokine release profiles, whereas when the initiating event is damaging in nature an increase in cell death is observed.

Within the realm of MS research, it would be interesting to continue this line of research to determine what effects, if any, the increased cytokine profile or increased oligodendrocyte cell death would have on the level of myelination and resulting neuronal health in a direct contact co-culture. We hypothesize that increasing the understanding of the synergistic effects of these pathways and the methods by which such cross talk occurs will help us to more accurately discover and create disease-modifying treatments for MS.

CHAPTER FIVE

CONCLUSION

Multiple Sclerosis is a debilitating disease for which no concrete causes have been isolated or identified. To date, the extent of the knowledge surrounding its aetiology are a variety of risk factors including genetics, geography, race, gender, and even early life viruses. However, it is not clear if one of the risk factors carries more importance than the others, whether the risk factors may work together in multiplicative ways to increase the likelihood of developing the disease, or even whether the various risk factors lead to different types of MS (in terms of disease type, disease course, and disease presentation).

In order to delve deeper in to the role of iron in MS disease progression, we took a translational approach, which included both clinical and cell culture work. Using a consistent patient pool we were able to suggest possible patterns of abnormal iron deposition in MS lesion, which may implicate maturity and/or severity of lesions to iron deposition. In addition to lesion severity being considered a factor in region-specific iron deposition, general disease severity also appears to affect the baseline iron load seen between patients. These results indicate a role for abnormal iron deposition in MS, so we then looked at cell culture to address mechanistic questions regarding iron regulation. Namely, we wanted to look into the potential mechanisms by which iron contributes to the pathology. As inflammation and demyelination are key pathological features of MS we specifically wanted to investigate the role of iron-related metabolic and signaling pathways in decreasing viability of oligodendrocytes. Seeing as HO-1 is a major player in the metabolism of heme iron, and is implicated in inflammatory cascades, we wanted to explore how dysregulation of this pathway may affect viability. Furthermore, due to the

bi-phasic role HO-1 can play we also wanted to determine whether synergistic effects existed between HO-1 and signaling pathways known to be involved in MS disease progression. Thus, in general we were looking for the cell culture work to corroborate the clinical findings and provide mechanistic insight into the potential contribution of iron to disease pathogenesis. We determined that a synergistic effect exists between the HO-1 pathway and the P2X family of receptors. Specifically, that they are correlated in the directionality of their effects; joint agonism lead to higher cell death in the oligodendrocyte pool, and conversely joint antagonism mitigated this effect. Of particular interest is how the manipulating these pathways in either a staggered or simultaneous manner induced varied responses from the microglia population in addition to varied levels of cell death in the oligodendrocyte population. The results presented here suggest that iron may not be the initiating factor in regards to lesion formation. However, based on the data that a more severe disease progression was linked to increased iron deposition, as well as the fact that activation of the HO-1 pathway in the presence of unresolved inflammation increased cell death, our data suggests that iron may play a causal role in determining the severity of the lesions.

New imaging techniques have greatly advanced our knowledge of iron localization both temporally with disease progression, as well as locally within various brain regions. However, these new techniques lack the ability to be able to visualize Type III lesions (which are found solely in the cortex). Type III lesions are particularly interesting as they are found predominantly in the gray matter, yet MS is a disease that is said to affect the myelin (white matter). Thus, the mechanisms behind their existence and their role towards disease progression remain very poorly understood.

The inability to effectively visualize Type III lesions creates an inability to determine how they may associate with disease progression, as well as how excess iron deposition may correlate with lesion severity/development. We reported interesting discrepancies in our data (Chapter 2) regarding the patterns of iron deposition compared to the reported existence of lesions post-mortem. Specifically, we found that lesions reported in the post-mortem reports were sometimes associated with increased levels of iron deposition. Additionally, regions in which no lesions were reported also exhibited increased levels of iron deposition. Due to the lack of knowledge surrounding the mechanisms behind the increased iron deposition within MS it is difficult to determine how this discrepancy in iron deposition vs. lesion location may affect disease progression. However, our hypothesis is that this discrepancy may be attributed to the inability to effectively visualize Type III lesions in conjunction with the fact that chronic lesions appear to lose the increased iron deposition. Therefore, the iron deposition not associated with the reported lesions may in fact be associated with the unreported active Type III lesions. We feel that investigating the potential relationship between iron deposition and Type III lesions would greatly increase our understanding of the role iron plays in disease progression.

It is important to remember that the accumulation of these results are the product of operating under the assumption that the various iron deposition patterns observed in Chapter Two are due to a causal relationship. In order to verify this, a larger patient pool is required. Thus, a huge limiting factor in the research presented here is that no causal relationship could be established between both lesion severity and disease severity with abnormal patterns of iron deposition. However, we believe that in order to establish this

essential causal link, preliminary research such as the work outlined in this thesis is required.

In the third chapter, in addition to describing a synergistic effect of the two pathways, the relevance of microglial activation via either DAMPs or PAMPs to the deleterious effects of the HO-1 pathway on oligodendrocytes was elucidated. This is supported by the data in (Hemin + ATP temporal resolution). As mentioned previously, ATP is a DAMP, whereas IFN is an initial receptor for the PAMP signaling cascade. Therefore ATP pre-treatment represents activation of MG with a DAMP, and IFN pre-treatment represents activation of MG with a PAMP. The altered ability of PAMP activation over DAMP activation to render the effects of the HO-1 pathway as toxic to the affected oligodendrocyte pool may correlate a non-resolved early-life virus with implication in the aetiology and disease progression of MS. Furthermore, this may also indicate that an association of altered of iron metabolism with the risk factor of early life viruses. However, it is not clear if any early -life virus may be sufficient to produce the increased risk of developing MS later in life, or if it is the contraction of a specific virus in conjunction with the inability to efficiently fight and clear the resulting inflammation are both required to cause the observed risk.

As previously discussed the role of excess iron deposition in the disease progression of MS is not understood. A main enzyme involved in the metabolic pathway of iron is HO-1. Under normal physiological circumstances HO-1 plays a trophic role and is associated with cytoprotection against stress stimuli. However, the data put forth here corroborates previous literature describing the ability of pathological circumstances to swing the effects of HO-1 from trophic to toxic. Indeed, when the agonism of the HO-1

pathway was paired with an activation pattern (using a DAMP) mimicking co-incident microglial activation, increased levels of cell death were observed in the associated oligodendrocyte pool. This seemingly bi-phasic effect of HO-1 may be linked to the hypo-cellularity observed in chronic lesions. That is, the chronic inflammation that is associated with MS may affect the activity of the HO-1 pathway so that is becomes toxic. This result would likely be observed in locations where excess iron is located, one of which being active MS lesions. Therefore it may be that the observed hypocellularity in chronic lesions (whereas no such hypocellularity is observed in active lesions) is due to the inability to resolve inflammation thereby rendering the HO-1 pathway toxic, ultimately leading to intra-lesional cell death.

Overall the findings put forth in this thesis suggest that any further work done with regards to excess iron deposition in patients with MS need to take the inter-patient variability into consideration. Furthermore, contiguous patient pools are essential for any causal relationships to be determined from the latter patient pool. In addition to the patient work previously mentioned, the characterization of the TR33B cells opens up avenues of more applicable cell research. Oligodendrocytes are implicated in a wide variety of pathologies: from neurodegeneration in Alzheimer's disease to psychiatric pathologies such as schizophrenia. Therefore the characterization of a commercially available rat oligodendrocyte line allows the breadth and depth of questions asked by the scientific community to broaden in regards to such pathologies.

Future Directions

In order to verify the causal nature between the various aspects of disease progression and abnormal iron deposition we would be interested in obtaining more subjects and performing the same set of experiments on them. In addition, quantifying the

intensity of the iron staining using the image analysis program would also be of interest with a larger patient pool. It would be of further interest to apply the same drug-treatment regimen to the direct neuron-glia contact co-culture outlined in Chapter Three to observe if myelination is affected. Specifically, we would be interested in determining if a reduction of myelin is observed, if this sensitizes the neurons to minor insults thereby resulting in the Wallerian degeneration that is poorly understood in MS. By the same token, we would also be interested in ascertaining the role ferroptosis may be playing in the role of degeneration and inflammation in MS. We hypothesize that a combination of regulated cell death pathways create the cell death and degeneration observed in MS. Therefore, in addition to the apoptosis observed within the oligodendrocyte pool in Chapter 4, it would be of interest to determine if ferroptosis would create an additional mechanism of cell death. Given that excess intracellular iron is largely associated with the mitochondria and mitochondrial dysregulation has been associated with MS, it would also be interesting to test mitochondrial metabolism in response to the drug treatment regimen outlined in Chapter 4.

The question of how excess iron is either a cause or result of the pathological circumstances in MS is being widely investigated. It is suggested here that great patient-specific variability exists with regards to the concentration and pattern of excess iron deposition, and that this variability may be linked to the various presentations of MS. In addition, the ability of iron to confer toxic effects may be associated with the nature and time-span of the initiating immune insult. Specifically unresolved, pathogen-initiated, immune insults may create the environment changes necessary to prompt a toxic change to iron homeostasis.

1. Ann Piertrangelo and Valencia Higuera. Multiple Sclerosis by the Numbers: Facts, Statistics, and You. *Healthline* Available at: http://www.healthline.com/health/multiple-sclerosis/facts-statistics-infographic.
2. MS Prevalence. *National Multiple Sclerosis Society* Available at: http://www.nationalmssociety.org/About-the-Society/MS-Prevalence.
3. About MS. *Multiple Sclerosis Society of Canada* Available at: https://mssociety.ca/about-ms.
4. James A. Wilson. Brain Imaging in Multiple Sclerosis. *Medscape* (2016). Available at: http://emedicine.medscape.com/article/342254-overview.
5. Filippi, M. & Rocca, M. A. MR Imaging of Multiple Sclerosis. *Radiology* **259,** 659–681 (2011).
6. Ge, Y. Multiple sclerosis: the role of MR imaging. *AJNR Am. J. Neuroradiol.* **27,** 1165–1176 (2006).
7. Weissert, R. The Immune Pathogenesis of Multiple Sclerosis. *J. Neuroimmune Pharmacol.* **8,** 857–866 (2013).
8. Wu, G. F. & Alvarez, E. The Immunopathophysiology of Multiple Sclerosis. *Neurol. Clin.* **29,** 257–278 (2011).
9. Lassmann, H. The pathology of multiple sclerosis and its evolution. *Philos. Trans. R. Soc. B Biol. Sci.* **354,** 1635–1640 (1999).
10. Todorich, B., Pasquini, J. M., Garcia, C. I., Paez, P. M. & Connor, J. R. Oligodendrocytes and myelination: the role of iron. *Glia* **57,** 467–478 (2009).
11. Dixon, S. J. & Stockwell, B. R. The role of iron and reactive oxygen species in cell death. *Nat. Chem. Biol.* **10,** 9–17 (2014).

12. Batista-Nascimento, L., Pimentel, C., Andrade Menezes, R. & Rodrigues-Pousada, C. Iron and Neurodegeneration: From Cellular Homeostasis to Disease. *Oxid. Med. Cell. Longev.* **2012,** 1–8 (2012).
13. Xu, W., Barrientos, T. & Andrews, N. C. Iron and Copper in Mitochondrial Diseases. *Cell Metab.* **17,** 319–328 (2013).
14. Walter, P. B. *et al.* Iron deficiency and iron excess damage mitochondria and mitochondrial DNA in rats. *Proc. Natl. Acad. Sci.* **99,** 2264–2269 (2002).
15. LeVine, S. M. Iron deposits in multiple sclerosis and Alzheimer's disease brains. *Brain Res.* **760,** 298–303 (1997).
16. Wood, H. Alzheimer disease: Iron--the missing link between ApoE and Alzheimer disease? *Nat. Rev. Neurol.* **11,** 369 (2015).
17. Salkovic-Petrisic, M. *et al.* Multi-target iron-chelators improve memory loss in a rat model of sporadic Alzheimer's disease. *Life Sci.* **136,** 108–119 (2015).
18. Pretorius, E., Bester, J. & Kell, D. B. A Bacterial Component to Alzheimer's-Type Dementia Seen via a Systems Biology Approach that Links Iron Dysregulation and Inflammagen Shedding to Disease. *J. Alzheimers Dis. JAD* **53,** 1237–1256 (2016).
19. Peters, D. G., Connor, J. R. & Meadowcroft, M. D. The relationship between iron dyshomeostasis and amyloidogenesis in Alzheimer's disease: Two sides of the same coin. *Neurobiol. Dis.* **81,** 49–65 (2015).
20. Moon, Y., Han, S.-H. & Moon, W.-J. Patterns of Brain Iron Accumulation in Vascular Dementia and Alzheimer's Dementia Using Quantitative Susceptibility Mapping Imaging. *J. Alzheimers Dis. JAD* **51,** 737–745 (2016).

21. Ayton, S., Faux, N. G., Bush, A. I. & Alzheimer's Disease Neuroimaging Initiative. Ferritin levels in the cerebrospinal fluid predict Alzheimer's disease outcomes and are regulated by APOE. *Nat. Commun.* **6,** 6760 (2015).

22. Xu, H.-M., Wang, J., Song, N., Jiang, H. & Xie, J.-X. [Glial cells are involved in iron accumulation and degeneration of dopamine neurons in Parkinson's disease]. *Sheng Li Xue Bao* **68,** 455–463 (2016).

23. Jiao, J. *et al.* Meta-analysis of the association between serum iron levels and Parkinson's disease: Evidence from 11 publications. *Brain Res.* **1646,** 490–493 (2016).

24. Wang, J.-Y. *et al.* Meta-analysis of brain iron levels of Parkinson's disease patients determined by postmortem and MRI measurements. *Sci. Rep.* **6,** 36669 (2016).

25. Peckham, M. E. *et al.* Novel Pattern of Iron Deposition in the Fascicula Nigrale in Patients with Parkinson's Disease: A Pilot Study. *Radiol. Res. Pract.* **2016,** 9305018 (2016).

26. Lu, L.-N., Qian, Z.-M., Wu, K.-C., Yung, W.-H. & Ke, Y. Expression of Iron Transporters and Pathological Hallmarks of Parkinson's and Alzheimer's Diseases in the Brain of Young, Adult, and Aged Rats. *Mol. Neurobiol.* (2016). doi:10.1007/s12035-016-0067-0

27. Lan, A. P., Chen, J., Chai, Z. F. & Hu, Y. The neurotoxicity of iron, copper and cobalt in Parkinson's disease through ROS-mediated mechanisms. *Biometals Int. J. Role Met. Ions Biol. Biochem. Med.* **29,** 665–678 (2016).

28. Guan, X. *et al.* Influence of regional iron on the motor impairments of Parkinson's disease: A quantitative susceptibility mapping study. *J. Magn. Reson. Imaging JMRI* (2016). doi:10.1002/jmri.25434

29. Deng, Q. *et al.* Lower hemoglobin levels in patients with parkinson's disease are associated with disease severity and iron metabolism. *Brain Res.* (2016). doi:10.1016/j.brainres.2016.11.007

30. Aguirre, P. *et al.* Neuroprotective effect of a new 7,8-dihydroxycoumarin-based Fe2+/Cu2+ chelator in cell and animal models of Parkinson's disease. *ACS Chem. Neurosci.* (2016). doi:10.1021/acschemneuro.6b00309

31. Van Bergen, J. M. G. *et al.* Quantitative Susceptibility Mapping Suggests Altered Brain Iron in Premanifest Huntington Disease. *AJNR Am. J. Neuroradiol.* **37,** 789–796 (2016).

32. Sánchez-Castañeda, C. *et al.* The role of iron in gray matter degeneration in Huntington's disease: a magnetic resonance imaging study. *Hum. Brain Mapp.* **36,** 50–66 (2015).

33. Muller, M. & Leavitt, B. R. Iron dysregulation in Huntington's disease. *J. Neurochem.* **130,** 328–350 (2014).

34. Macerollo, A. *et al.* Susceptibility-weighted imaging changes suggesting brain iron accumulation in Huntington's disease: an epiphenomenon which causes diagnostic difficulty. *Eur. J. Neurol.* **21,** e16–17 (2014).

35. Domínguez, J. F. D. *et al.* Iron accumulation in the basal ganglia in Huntington's disease: cross-sectional data from the IMAGE-HD study. *J. Neurol. Neurosurg. Psychiatry* **87,** 545–549 (2016).

36. Di Paola, M. *et al.* MRI measures of corpus callosum iron and myelin in early Huntington's disease. *Hum. Brain Mapp.* **35,** 3143–3151 (2014).

37. Chen, J. *et al.* Iron accumulates in Huntington's disease neurons: protection by deferoxamine. *PloS One* **8,** e77023 (2013).

38. Berggren, K. L. *et al.* Neonatal Iron Supplementation Induces Striatal Atrophy in Female YAC128 Huntington's Disease Mice. *J. Huntingt. Dis.* **5,** 53–63 (2016).

39. Berggren, K. L. *et al.* Neonatal iron supplementation potentiates oxidative stress, energetic dysfunction and neurodegeneration in the R6/2 mouse model of Huntington's disease. *Redox Biol.* **4,** 363–374 (2015).

40. Yazar, M. S., Fistikci, N., Balaban, O. D., Eradamlar, N. & Alpkan, L. Psychotic Disorder in Neurodegeneration with Brain Iron Accumulation. *Clin. Schizophr. Relat. Psychoses* **10,** 178–180 (2016).

41. Salomão, R. P. A. *et al.* A diagnostic approach for neurodegeneration with brain iron accumulation: clinical features, genetics and brain imaging. *Arq. Neuropsiquiatr.* **74,** 587–596 (2016).

42. Mehnaaz, L. Neurodegeneration with brain iron accumulation (NBIA) formerly Hallervorden- Spatz disease. *J. Assoc. Physicians India* **64,** 132 (2016).

43. Limongi, J. C. P. Neurodegeneration with brain iron accumulation. *Arq. Neuropsiquiatr.* **74,** 517–518 (2016).

44. P, H. M. & Timothy, G. J. Mitochondrial Iron Metabolism and Its Role in Neurodegeneration. *J. Alzheimers Dis.* 551–568 (2010). doi:10.3233/JAD-2010-100354

45. Modica, C. M. *et al.* Iron and Volume in the Deep Gray Matter: Association with Cognitive Impairment in Multiple Sclerosis. *Am. J. Neuroradiol.* **36,** 57–62 (2015).

46. Hametner, S. *et al.* Iron and neurodegeneration in the multiple sclerosis brain: Iron in the MS Brain. *Ann. Neurol.* **74,** 848–861 (2013).

47. Haider, L. *et al.* Multiple sclerosis deep grey matter: the relation between demyelination, neurodegeneration, inflammation and iron. *J. Neurol. Neurosurg. Psychiatry* (2014). doi:10.1136/jnnp-2014-307712

48. Haider, L. Inflammation, Iron, Energy Failure, and Oxidative Stress in the Pathogenesis of Multiple Sclerosis. *Oxid. Med. Cell. Longev.* **2015,** 725370 (2015).

49. Craelius, W., Migdal, M. W., Luessenhop, C. P., Sugar, A. & Mihalakis, I. Iron deposits surrounding multiple sclerosis plaques. *Arch. Pathol. Lab. Med.* **106,** 397–399 (1982).

50. Blazejewska, A. I. *et al.* Increase in the iron content of the substantia nigra and red nucleus in multiple sclerosis and clinically isolated syndrome: A 7 Tesla MRI study: Iron Increase in the SN & RN in MS & CIS. *J. Magn. Reson. Imaging* **41,** 1065–1070 (2015).

51. Zivadinov, R., Weinstock-Guttman, B. & Pirko, I. Iron deposition and inflammation in multiple sclerosis. Which one comes first? *BMC Neurosci.* **12,** 60 (2011).

52. Williams, R., Buchheit, C. L., Berman, N. E. J. & LeVine, S. M. Pathogenic implications of iron accumulation in multiple sclerosis: Iron deposition in multiple sclerosis. *J. Neurochem.* **120,** 7–25 (2012).

53. Williams, R. *et al.* Iron deposition is independent of cellular inflammation in a cerebral model of multiple sclerosis. *BMC Neurosci.* **12,** 59 (2011).

54. Mehta, V. *et al.* Iron Is a Sensitive Biomarker for Inflammation in Multiple Sclerosis Lesions. *PLoS ONE* **8,** e57573 (2013).

55. Levine, S. M. & Chakrabarty, A. The Role of Iron in the Pathogenesis of Experimental Allergic Encephalomyelitis and Multiple Sclerosis. *Ann. N. Y. Acad. Sci.* **1012,** 252–266 (2004).

56. Bagnato, F. *et al.* Tracking iron in multiple sclerosis: a combined imaging and histopathological study at 7 Tesla. *Brain* **134,** 3602–3615 (2011).

57. Raz, E. *et al.* Relationship between iron accumulation and white matter injury in multiple sclerosis: a case–control study. *J. Neurol.* **262,** 402–409 (2015).

58. Valberg, L. S., Flanagan, P. R., Kertesz, A. & Ebers, G. C. Abnormalities in iron metabolism in multiple sclerosis. *Can. J. Neurol. Sci. J. Can. Sci. Neurol.* **16,** 184–186 (1989).

59. Singh, N. *et al.* Brain Iron Homeostasis: From Molecular Mechanisms To Clinical Significance and Therapeutic Opportunities. *Antioxid. Redox Signal.* **20,** 1324–1363 (2014).

60. Walsh, A. J. *et al.* Longitudinal MR imaging of iron in multiple sclerosis: an imaging marker of disease. *Radiology* **270,** 186–196 (2014).

61. Bo, L., Geurts, J. J. G., Mork, S. J. & Valk, P. Grey matter pathology in multiple sclerosis. *Acta Neurol. Scand.* **113,** 48–50 (2006).

62. Richardson, D. R. *et al.* Mitochondrial iron trafficking and the integration of iron metabolism between the mitochondrion and cytosol. *Proc. Natl. Acad. Sci.* **107,** 10775–10782 (2010).

63. Levi, S. & Rovida, E. The role of iron in mitochondrial function. *Biochim. Biophys. Acta BBA - Gen. Subj.* **1790,** 629–636 (2009).

64. Kalman, B. Role of mitochondria in multiple sclerosis. *Curr. Neurol. Neurosci. Rep.* **6,** 244–252 (2006).

65. Mao, P. & Reddy, P. H. Is multiple sclerosis a mitochondrial disease? *Biochim. Biophys. Acta BBA - Mol. Basis Dis.* **1802,** 66–79 (2010).

66. Dixon, S. J. *et al.* Ferroptosis: an iron-dependent form of nonapoptotic cell death. *Cell* **149,** 1060–1072 (2012).

67. Cao, J. Y. & Dixon, S. J. Mechanisms of ferroptosis. *Cell. Mol. Life Sci. CMLS* **73,** 2195–2209 (2016).

68. Do Van, B. *et al.* Ferroptosis, a newly characterized form of cell death in Parkinson's disease that is regulated by PKC. *Neurobiol. Dis.* **94,** 169–178 (2016).

69. Gao, M. *et al.* Ferroptosis is an autophagic cell death process. *Cell Res.* **26,** 1021–1032 (2016).

70. Hou, W. *et al.* Autophagy promotes ferroptosis by degradation of ferritin. *Autophagy* **12,** 1425–1428 (2016).

71. Wu, D. & Chen, L. Ferroptosis: a novel cell death form will be a promising therapy target for diseases. *Acta Biochim. Biophys. Sin.* **47,** 857–859 (2015).

72. Xie, Y. *et al.* Ferroptosis: process and function. *Cell Death Differ.* **23,** 369–379 (2016).

73. Yang, W. S. & Stockwell, B. R. Ferroptosis: Death by Lipid Peroxidation. *Trends Cell Biol.* **26,** 165–176 (2016).

74. Kwon, M.-Y., Park, E., Lee, S.-J. & Chung, S. W. Heme oxygenase-1 accelerates erastin-induced ferroptotic cell death. *Oncotarget* **6,** 24393–24403 (2015).

75. Gulcher, J. R., Vartanian, T. & Stefansson, K. Is multiple sclerosis an autoimmune disease? *Clin. Neurosci. N. Y. N* **2,** 246–252 (1994).

76. Wootla, B., Eriguchi, M. & Rodriguez, M. Is Multiple Sclerosis an Autoimmune Disease? *Autoimmune Dis.* **2012,** 1–12 (2012).

77. Chaudhuri, A. Multiple sclerosis: looking beyond autoimmunity. *J. R. Soc. Med.* **98,** 303–306 (2005).

78. Höftberger, R., Leisser, M., Bauer, J. & Lassmann, H. Autoimmune encephalitis in humans: how closely does it reflect multiple sclerosis ? *Acta Neuropathol. Commun.* **3,** (2015).

79. Cepok, S. *et al.* Identification of Epstein-Barr virus proteins as putative targets of the immune response in multiple sclerosis. *J. Clin. Invest.* **115,** 1352–1360 (2005).

80. Handel, A. E. *et al.* An updated meta-analysis of risk of multiple sclerosis following infectious mononucleosis. *PloS One* **5,** (2010).

81. Thacker, E. L., Mirzaei, F. & Ascherio, A. Infectious mononucleosis and risk for multiple sclerosis: a meta-analysis. *Ann. Neurol.* **59,** 499–503 (2006).

82. Dooley, M. M., de Gannes, S. L., Fu, K. A. & Lindsey, J. W. The increased antibody response to Epstein-Barr virus in multiple sclerosis is restricted to selected virus proteins. *J. Neuroimmunol.* **299,** 147–151 (2016).

83. Van der Star, B. J. *et al.* In vitro and in vivo models of multiple sclerosis. *CNS Neurol. Disord. Drug Targets* **11,** 570–588 (2012).

84. Hiraishi, H. *et al.* Role for iron in reactive oxygen species-mediated cytotoxicity to cultured rat gastric mucosal cells. *Am. J. Physiol.* **260,** G556–563 (1991).

85. Gammella, E., Recalcati, S. & Cairo, G. Dual Role of ROS as Signal and Stress Agents: Iron Tips the Balance in favor of Toxic Effects. *Oxid. Med. Cell. Longev.* **2016,** 1–9 (2016).

86. Walsh, A. J. *et al.* Multiple sclerosis: validation of MR imaging for quantification and detection of iron. *Radiology* **267,** 531–542 (2013).

87. Wessling-Resnick, M. Iron Homeostasis and the Inflammatory Response. *Annu. Rev. Nutr.* **30,** 105–122 (2010).

88. Merrill, J. E. In Vitro and In Vivo Pharmacological Models to Assess Demyelination and Remyelination. *Neuropsychopharmacology* **34,** 55–73 (2009).

89. Göbel, K. *et al.* An ex vivo model of an oligodendrocyte-directed T-cell attack in acute brain slices. *J. Vis. Exp. JoVE* (2015). doi:10.3791/52205

90. Davis, H. *et al.* A phenotypic culture system for the molecular analysis of CNS myelination in the spinal cord. *Biomaterials* **35,** 8840–8845 (2014).

91. Davis, H. *et al.* Rat Cortical Oligodendrocyte-Embryonic Motoneuron Co-Culture: An In Vitro Axon-Oligodendrocyte Interaction Model. *J. Biomater. Tissue Eng.* **2,** 206–214 (2012).

92. Li, S., Vana, A. C., Ribeiro, R. & Zhang, Y. Distinct role of nitric oxide and peroxynitrite in mediating oligodendrocyte toxicity in culture and in experimental autoimmune encephalomyelitis. *Neuroscience* **184,** 107–119 (2011).

93. Iannaccone, P. M. & Jacob, H. J. Rats! *Dis. Model. Mech.* **2,** 206–210 (2009).

94. Horiuchi, M., Lindsten, T., Pleasure, D. & Itoh, T. Differing in vitro survival dependency of mouse and rat NG2 $^{+}$ oligodendroglial progenitor cells. *J. Neurosci. Res.* NA–NA (2009). doi:10.1002/jnr.22262

95. Pockley, A. G. & Bolton, A. E. Placental protein 14 (PP14) inhibits the synthesis of interleukin-2 and the release of soluble interleukin-2 receptors from phytohaemagglutinin-stimulated lymphocytes. *Clin. Exp. Immunol.* **77,** 252–256 (1989).

96. Pedraza, C. E. *et al.* Induction of Oligodendrocyte Differentiation and In Vitro Myelination by Inhibition of Rho-Associated Kinase. *ASN Neuro* **6,** (2014).

97. Lourenço, T. *et al.* Modulation of oligodendrocyte differentiation and maturation by combined biochemical and mechanical cues. *Sci. Rep.* **6,** 21563 (2016).

98. Chen, Y. *et al.* Isolation and culture of rat and mouse oligodendrocyte precursor cells. *Nat. Protoc.* **2,** 1044–1051 (2007).

99. Chojnacki, A. & Weiss, S. Production of neurons, astrocytes and oligodendrocytes from mammalian CNS stem cells. *Nat. Protoc.* **3,** 935–940 (2008).

100. Life Technologies, 2015. Differentiating Glial Precursor Cells into Astrocytes and Oligodendrocytes. Available at: https://www.lifetechnologies.com/ca/en/home/references/protocols/neurobiology/neurobiology-protocols/differentiating-glial-precursor-cells-into-astrocytes-and-oligodendrocytes.html.

101. Differentiating Neural Stem Cells in Neurons and Glial Cells. *Thermo Fisher Scientific* (2011). Available at: https://www.thermofisher.com/ca/en/home/references/protocols/neurobiology/neurob

iology-protocols/differentiating-neural-stem-cells-into-neurons-and-glial-cells.html. (Accessed: 13th September 2016)

102. Sher, F. *et al.* Differentiation of Neural Stem Cells into Oligodendrocytes: Involvement of the Polycomb Group Protein Ezh2. *Stem Cells* **26,** 2875–2883 (2008).

103. Neural Stem Cells. *Stem Cell Technologies* (2015). Available at: https://www.stemcell.com/neural-stem-cells-lp.html. (Accessed: 13th September 2016)

104. Louis, S. A., Mak, C. K. H. & Reynolds, B. A. in *Basic Cell Culture Protocols* (eds. Helgason, C. D. & Miller, C. L.) **946,** 479–506 (Humana Press, 2013).

105. Fields, K. L., Gosling, C., Megson, M. & Stern, P. L. New cell surface antigens in rat defined by tumors of the nervous system. *Proc. Natl. Acad. Sci. U. S. A.* **72,** 1296–1300 (1975).

106. TR33B. *Sigma-Aldrich* Available at: http://www.sigmaaldrich.com/catalog/product/sigma/85040102?lang=en&region=CA. (Accessed: 13th September 2016)

107. Dhami, K. S., Churchward, M. A., Baker, G. B. & Todd, K. G. Fluoxetine and citalopram decrease microglial release of glutamate and D-serine to promote cortical neuronal viability following ischemic insult. *Mol. Cell. Neurosci.* **56,** 365–374 (2013).

108. Girolamo, F. *et al.* Characterization of oligodendrocyte lineage precursor cells in the mouse cerebral cortex: a confocal microscopy approach to demyelinating diseases. *Ital. J. Anat. Embryol. Arch. Ital. Anat. Ed Embriologia* **115,** 95–102 (2010).

109. Nave, K.-A. & Ehrenreich, H. Myelination and oligodendrocyte functions in psychiatric diseases. *JAMA Psychiatry* **71,** 582–584 (2014).

110. Garman, R. H. Histology of the Central Nervous System. *Toxicol. Pathol.* **39,** 22–35 (2011).

111. Learmonth, Y. C., Pilutti, L. A. & Motl, R. W. Generalised cognitive motor interference in multiple sclerosis. *Gait Posture* **42,** 96–100 (2015).

112. Cerasa, A. *et al.* MR imaging and cognitive correlates of relapsing-remitting multiple sclerosis patients with cerebellar symptoms. *J. Neurol.* **260,** 1358–1366 (2013).

113. Gil Moreno, M. J. *et al.* Neuropsychological syndromes in multiple sclerosis. *Psicothema* **25,** 452–460 (2013).

114. Bjelobaba, I., Savic, D. & Lavrnja, I. Multiple sclerosis and neuroinflammation: The overview of current and prospective therapies. *Curr. Pharm. Des.* (2016).

115. Brownlee, W. J., Hardy, T. A., Fazekas, F. & Miller, D. H. Diagnosis of multiple sclerosis: progress and challenges. *Lancet Lond. Engl.* (2016). doi:10.1016/S0140-6736(16)30959-X

116. Reale, M. & Sánchez-Ramón, S. Lipids at the Cross-road of Autoimmunity in Multiple Sclerosis. *Curr. Med. Chem.* (2016).

117. Zhang, W. *et al.* Role and Mechanism of Microglial Activation in Iron-Induced Selective and Progressive Dopaminergic Neurodegeneration. *Mol. Neurobiol.* **49,** 1153–1165 (2014).

118. Streit, W. J. Microglia as neuroprotective, immunocompetent cells of the CNS. *Glia* **40,** 133–139 (2002).

119. Nayak, D., Roth, T. L. & McGavern, D. B. Microglia Development and Function*. *Annu. Rev. Immunol.* **32,** 367–402 (2014).

120. Dziedzic, T. *et al.* Wallerian Degeneration: A Major Component of Early Axonal Pathology in Multiple Sclerosis: Wallerian degeneration in MS. *Brain Pathol.* no–no (2010). doi:10.1111/j.1750-3639.2010.00401.x

121. Haines, J. D., Inglese, M. & Casaccia, P. Axonal Damage in Multiple Sclerosis. *Mt. Sinai J. Med. J. Transl. Pers. Med.* **78,** 231–243 (2011).

122. Zeis, T. & Schaeren-Wiemers, N. Lame ducks or fierce creatures? The role of oligodendrocytes in multiple sclerosis. *J. Mol. Neurosci. MN* **35,** 91–100 (2008).

123. Baumann, N. & Pham-Dinh, D. Biology of oligodendrocyte and myelin in the mammalian central nervous system. *Physiol. Rev.* **81,** 871–927 (2001).

124. Patel, J. & Balabanov, R. Molecular Mechanisms of Oligodendrocyte Injury in Multiple Sclerosis and Experimental Autoimmune Encephalomyelitis. *Int. J. Mol. Sci.* **13,** 10647–10659 (2012).

125. Dheen, S. T., Kaur, C. & Ling, E.-A. Microglial activation and its implications in the brain diseases. *Curr. Med. Chem.* **14,** 1189–1197 (2007).

126. Eyo, U. B. & Dailey, M. E. Microglia: key elements in neural development, plasticity, and pathology. *J. Neuroimmune Pharmacol. Off. J. Soc. NeuroImmune Pharmacol.* **8,** 494–509 (2013).

127. Boche, D., Perry, V. H. & Nicoll, J. A. R. Review: activation patterns of microglia and their identification in the human brain. *Neuropathol. Appl. Neurobiol.* **39,** 3–18 (2013).

128. Kitamura, Y. *et al.* Intracerebroventricular injection of microglia protects against focal brain ischemia. *J. Pharmacol. Sci.* **94,** 203–206 (2004).

129. Town, T., Nikolic, V. & Tan, J. The microglial 'activation' continuum: from innate to adaptive responses. *J. Neuroinflammation* **2,** 24 (2005).

130. Lull, M. E. & Block, M. L. Microglial activation and chronic neurodegeneration. *Neurotherapeutics* **7,** 354–365 (2010).

131. Nakamura, Y. Regulating factors for microglial activation. *Biol. Pharm. Bull.* **25,** 945–953 (2002).

132. Tozaki-Saitoh, H., Tsuda, M. & Inoue, K. [Purinergic regulation of microglia]. *Nihon Yakurigaku Zasshi Folia Pharmacol. Jpn.* **136,** 93–97 (2010).

133. Sperlágh, B. & Illes, P. Purinergic modulation of microglial cell activation. *Purinergic Signal.* **3,** 117–127 (2007).

134. Rayah, A., Kanellopoulos, J. M. & Di Virgilio, F. P2 receptors and immunity. *Microbes Infect. Inst. Pasteur* **14,** 1254–1262 (2012).

135. Vázquez-Villoldo, N. *et al.* P2X4 receptors control the fate and survival of activated microglia. *Glia* **62,** 171–184 (2014).

136. Tozaki-Saitoh, H., Tsuda, M. & Inoue, K. Role of purinergic receptors in CNS function and neuroprotection. *Adv. Pharmacol. San Diego Calif* **61,** 495–528 (2011).

137. Monif, M., Burnstock, G. & Williams, D. A. Microglia: proliferation and activation driven by the P2X7 receptor. *Int. J. Biochem. Cell Biol.* **42,** 1753–1756 (2010).

138. Grygorowicz, T., Sulejczak, D. & Struzynska, L. Expression of purinergic P2X7 receptor in rat brain during the symptomatic phase of experimental autoimmune

encephalomyelitis and after recovery of neurological deficits. *Acta Neurobiol. Exp. (Warsz.)* **71,** 65–73 (2011).

139. Grygorowicz, T., Struzyńska, L., Sulkowski, G., Chalimoniuk, M. & Sulejczak, D. Temporal expression of P2X7 purinergic receptor during the course of experimental autoimmune encephalomyelitis. *Neurochem. Int.* **57,** 823–829 (2010).

140. Caragnano, M. *et al.* Monocytes P2X7 purinergic receptor is modulated by glatiramer acetate in multiple sclerosis. *J. Neuroimmunol.* **245,** 93–97 (2012).

141. Coddou, C., Yan, Z., Obsil, T., Huidobro-Toro, J. P. & Stojilkovic, S. S. Activation and regulation of purinergic P2X receptor channels. *Pharmacol. Rev.* **63,** 641–683 (2011).

142. Matute, C. *et al.* P2X(7) receptor blockade prevents ATP excitotoxicity in oligodendrocytes and ameliorates experimental autoimmune encephalomyelitis. *J. Neurosci. Off. J. Soc. Neurosci.* **27,** 9525–9533 (2007).

143. Sharp, A. J. *et al.* P2x7 deficiency suppresses development of experimental autoimmune encephalomyelitis. *J. Neuroinflammation* **5,** 33 (2008).

144. Oyanguren-Desez, O. *et al.* Gain-of-function of P2X7 receptor gene variants in multiple sclerosis. *Cell Calcium* **50,** 468–472 (2011).

145. Boumechache, M., Masin, M., Edwardson, J. M., Górecki, D. C. & Murrell-Lagnado, R. Analysis of assembly and trafficking of native P2X4 and P2X7 receptor complexes in rodent immune cells. *J. Biol. Chem.* **284,** 13446–13454 (2009).

146. Sakaki, H. *et al.* P2X4 receptor regulates P2X7 receptor-dependent IL-1β and IL-18 release in mouse bone marrow-derived dendritic cells. *Biochem. Biophys. Res. Commun.* **432,** 406–411 (2013).

147. Kawano, A. *et al.* Involvement of P2X4 receptor in P2X7 receptor-dependent cell death of mouse macrophages. *Biochem. Biophys. Res. Commun.* **419,** 374–380 (2012).

148. Craigie, E., Birch, R. E., Unwin, R. J. & Wildman, S. S. The relationship between P2X4 and P2X7: a physiologically important interaction? *Front. Physiol.* **4,** 216 (2013).

149. Casas-Pruneda, G., Reyes, J. P., Pérez-Flores, G., Pérez-Cornejo, P. & Arreola, J. Functional interactions between P2X4 and P2X7 receptors from mouse salivary epithelia. *J. Physiol.* **587,** 2887–2901 (2009).

150. Guo, C., Masin, M., Qureshi, O. S. & Murrell-Lagnado, R. D. Evidence for functional P2X4/P2X7 heteromeric receptors. *Mol. Pharmacol.* **72,** 1447–1456 (2007).

151. Benkovic, S. A. & Connor, J. R. Ferritin, transferrin, and iron in selected regions of the adult and aged rat brain. *J. Comp. Neurol.* **338,** 97–113 (1993).

152. Farina, M., Avila, D. S., da Rocha, J. B. T. & Aschner, M. Metals, oxidative stress and neurodegeneration: a focus on iron, manganese and mercury. *Neurochem. Int.* **62,** 575–594 (2013).

153. Gebril, O. H., Simpson, J. E., Kirby, J., Brayne, C. & Ince, P. G. Brain Iron Dysregulation and the Risk of Ageing White Matter Lesions. *NeuroMolecular Med.* **13,** 289–299 (2011).

154. Chawla, S. *et al.* Iron and Non-Iron-Related Characteristics of Multiple Sclerosis and Neuromyelitis Optica Lesions at 7T MRI. *AJNR Am. J. Neuroradiol.* **37,** 1223–1230 (2016).

155. Alfadda, A. A. & Sallam, R. M. Reactive Oxygen Species in Health and Disease. *J. Biomed. Biotechnol.* **2012,** 1–14 (2012).

156. Bijjem, K. R. V., Padi, S. S. V. & lal Sharma, P. Pharmacological activation of heme oxygenase (HO)-1/carbon monoxide pathway prevents the development of peripheral neuropathic pain in Wistar rats. *Naunyn. Schmiedebergs Arch. Pharmacol.* **386,** 79–90 (2013).

157. Hsieh, C.-H. *et al.* Simvastatin-Induced Heme Oxygenase-1 Increases Apoptosis of Neuro 2A Cells in Response to Glucose Deprivation. *Toxicol. Sci.* **101,** 112–121 (2007).

158. Loboda, A., Damulewicz, M., Pyza, E., Jozkowicz, A. & Dulak, J. Role of Nrf2/HO-1 system in development, oxidative stress response and diseases: an evolutionarily conserved mechanism. *Cell. Mol. Life Sci.* **73,** 3221–3247 (2016).

159. Wagener, F. A. D. T. G. Different Faces of the Heme-Heme Oxygenase System in Inflammation. *Pharmacol. Rev.* **55,** 551–571 (2003).

160. Stahnke, T., Stadelmann, C., Netzler, A., Brück, W. & Richter-Landsberg, C. Differential upregulation of heme oxygenase-1 (HSP32) in glial cells after oxidative stress and in demyelinating disorders. *J. Mol. Neurosci. MN* **32,** 25–37 (2007).

161. Schluesener, H. J. & Seid, K. Heme oxygenase-1 in lesions of rat experimental autoimmune encephalomyelitis and neuritis. *J. Neuroimmunol.* **110,** 114–120 (2000).

162. Mehindate, K. *et al.* Proinflammatory cytokines promote glial heme oxygenase-1 expression and mitochondrial iron deposition: implications for multiple sclerosis. *J. Neurochem.* **77,** 1386–1395 (2001).

163. Domercq, M. *et al.* P2X7 receptors mediate ischemic damage to oligodendrocytes. *Glia* **58,** 730–740 (2010).

164. Yu, J. *et al.* Heme Oxygenase-1/Carbon Monoxide-regulated Mitochondrial Dynamic Equilibrium Contributes to the Attenuation of Endotoxin-induced Acute Lung Injury in Rats and in Lipopolysaccharide-activated Macrophages: *Anesthesiology* 1 (2016). doi:10.1097/ALN.0000000000001333

165. Bharucha, A. E. *et al.* Effects of hemin on heme oxygenase-1, gastric emptying, and symptoms in diabetic gastroparesis. *Neurogastroenterol. Motil.* (2016). doi:10.1111/nmo.12874

166. Palipoch, S. *et al.* Heme oxygenase-1 alleviates alcoholic liver steatosis: histopathological study. *J. Toxicol. Pathol.* **29,** 7–15 (2016).

167. Ciesla, M. *et al.* Heme oxygenase-1 controls an HDAC4-miR-206 pathway of oxidative stress in rhabdomyosarcoma. *Cancer Res.* (2016). doi:10.1158/0008-5472.CAN-15-1883

168. Tseng, C.-K. *et al.* Human heme oxygenase 1 is a potential host cell factor against dengue virus replication. *Sci. Rep.* **6,** 32176 (2016).

169. Nobre, L. S., Jeremias, H., Romão, C. C. & Saraiva, L. M. Examining the antimicrobial activity and toxicity to animal cells of different types of CO-releasing molecules. *Dalton Trans. Camb. Engl. 2003* **45,** 1455–1466 (2016).

170. Wilkinson, W. J. & Kemp, P. J. The carbon monoxide donor, CORM-2, is an antagonist of ATP-gated, human P2X4 receptors. *Purinergic Signal.* **7,** 57–64 (2011).

171. Wilkinson, W. J. & Kemp, P. J. Carbon monoxide: an emerging regulator of ion channels: Carbon monoxide and ion channels. *J. Physiol.* **589,** 3055–3062 (2011).

172. Lai, A. Y. & Todd, K. G. Differential regulation of trophic and proinflammatory microglial effectors is dependent on severity of neuronal injury. *Glia* **56,** 259–270 (2008).

173. Lai, A. Y. & Todd, K. G. Hypoxia-activated microglial mediators of neuronal survival are differentially regulated by tetracyclines. *Glia* **53,** 809–816 (2006).

174. Cannella, B. & Raine, C. S. Multiple sclerosis: cytokine receptors on oligodendrocytes predict innate regulation. *Ann. Neurol.* **55,** 46–57 (2004).

175. Matsuoka, Y., Okazaki, M. & Kitamura, Y. Induction of inducible heme oxygenase (HO-1) in the central nervous system: is HO-1 helpful or harmful? *Neurotox. Res.* **1,** 113–117 (1999).

176. Matsuoka, Y. *et al.* Induction of heme oxygenase-1 and major histocompatibility complex antigens in transient forebrain ischemia. *J. Cereb. Blood Flow Metab. Off. J. Int. Soc. Cereb. Blood Flow Metab.* **18,** 824–832 (1998).

177. Wang, L.-F. *et al.* Knockout of ho-1 protects the striatum from ferrous iron-induced injury in a male-specific manner in mice. *Sci. Rep.* **6,** 26358 (2016).

178. Sharp, F. R., Zhan, X. & Liu, D.-Z. Heat shock proteins in the brain: role of Hsp70, Hsp 27, and HO-1 (Hsp32) and their therapeutic potential. *Transl. Stroke Res.* **4,** 685–692 (2013).